Title
APPLICATIONS OF OPTICAL SECOND HARMONIC GENERATION TO SURFACE SCIENCE

Author
Shen, Y.R.

Publication Date
1984-09-01

Lawrence Berkeley Laboratory
UNIVERSITY OF CALIFORNIA

Materials & Molecular Research Division

Submitted as a chapter in New Laser and Optical Investigations of Chemistry and Structure at Interfaces, R.B. Hall and A.B. Ellis, Eds., Verlag Chemie Publishers

APPLICATIONS OF OPTICAL SECOND HARMONIC GENERATION TO SURFACE SCIENCE

Y.R. Shen

September 1984

Prepared for the U.S. Department of Energy under Contract DE-AC03-76SF00098

DISCLAIMER

Submitted to New Laser and Optical Investigations of Chemistry and Structure at Interfaces, eds. R.B. Hall and Arthur B. Ellis

APPLICATIONS OF OPTICAL SECOND HARMONIC GENERATION TO SURFACE SCIENCE

Y. R. Shen

Department of Physics
University of California
Berkeley, California 94720

and

Materials and Molecular Research Division
Lawrence Berkeley Laboratory
Berkeley, California 94720

ABSTRACT

Optical second harmonic generation can be an effective tool for surface studies. In this paper, the basic theory for the process and a number of demonstrating experiments are reviewed. We show that the process has a submonolayer sensitivity, and an overall flexibility. It can be used to probe resonant transitions, molecular arrangement, molecular orientations, adsorption and desorption, surface local-field enhancement, and time-resolved surface dynamics, and is generally applicable to a surface or interface between any two centrosymmetric media. It has been employed in the studies of atomic and molecular adsorption on metal and semiconductor surfaces in ultrahigh vacuum as well as on metal, semiconductor and insulator surfaces in air and liquid.

I. INTRODUCTION

Recently, laser studies of surfaces have become a subject of great interest.[1] On the one hand, lasers have the capability of modifying surfaces and interfaces. Research on laser-induced annealing, alloying, and processing has attracted increasing attention. On the other hand, lasers can be used to probe surfaces and interfaces. Introduction of laser techniques for surface probing has significantly broadened the horizon of surface science research. This article concerns the latter aspect of laser applications to surface science.

In surface science, characterization of surfaces and interfaces is of central importance as it is essential for the understanding of all surface phenomena. To this end, various techniques have been developed in the past.[2] While most of them involve emission, adsorption, or scattering of massive particles, a few rely on optical probing. The optical methods have the advantage of being generally applicable to interfaces between two dense media, but their sensitivities are often limited. With the advance of laser technology, however, optical techniques have been greatly improved. In addition, a number of new optical probes have been invented, which offer some unique possibilities for surface studies. For example, resonant fluorescence and multiphoton ionization have been employed to measure angular, velocity, and internal energy distributions of molecules scattered or desorbed from a surface, and thereby obtain detailed information about the molecule-surface interaction.[3] Laser-induced desorption,[4] photoacoustic spectroscopy,[5] and photothermal deflection spectroscopy[6] have been used for spectroscopic studies of adsorbates and surface states. Considerable effort has also

been made in the development of surface probes based on nonlinear optical effects.

Both second-order and third-order nonlinear optical processes have been considered for surface studies. Coherent Raman spectroscopy is an example of the third-order processes. Stimulated Raman gain spectroscopy is known to have very high sensitivity, especially when continuously mode-locked lasers and synchronous detection schemes are used.[7] Detection of a gain as small as $\sim 10^{-8}$ is possible, and the technique has been shown to be sensitive enough to detect the Raman spectrum of a molecular monolayer.[8] Coherent anti-Stokes Raman spectroscopy (CARS) is also extremely sensitive, and should be capable of detecting a molecular monolayer.[9] The sensitivities of both Raman spectroscopies can be further enhanced by employing surface or guided optical waves as pump and probe. However, both also suffer from complexity of the experimental arrangement and from the undesired contribution to the signal from the substrate on which the molecules adsorb. Spectral selectivity is often the only basis that can be used to discriminate the adsorbed molecules against the substrate in this case.

Second-order nonlinear optical processes, when allowed, are generally much stronger than third-order processes, and are easily detectable even in a molecular monolayer. The experimental arrangement is also much simpler. It turns out that the second-order processes are particularly suitable for surface studies. They are surface-specific at interfaces between two media with inversion symmetry for the following reason. From a simple symmetry argument, it can be shown that a second-order process is forbidden in a centrosymmetric medium in the electric-

dipole approximation, but is necessarily allowed at a surface or interface. In this sense, the second-order processes hold an intrinsic surface specificity on the atomic scale.[10] The surface sensitivity of the second-order processes indeed has been demonstrated in a number of early experiments on surface second harmonic generation (SHG).[11] More recent work has been focused on exploiting the SHG process as a tool for surface studies.[12-16] The latter is the main theme of this review article.

There are two important criterions a viable new surface tool must satisfy. First, it must have enough sensitivity to detect a molecular monolayer or submonolayer. Second, it must have enough advantages over the existing surface probes. The second-order nonlinear optical processes are indeed sensitive enough to detect a molecular submonolayer. Their major advantages over the conventional surface surfaces are in the very high spectral resolution (< 0.01 cm^{-1}) and time resolution (< 1 psec) a nonlinear optical technique can offer, and in the fact that such processes can be used to study interfaces between two dense media. As we shall see in later sections, the various possible combinations of input and output polarizations also allow us to deduce information about the surface structural symmetry and the orientation of molecular adsorbates.

In the following sections, we first describe briefly the theoretical basis for SHG. We then selectively review the various experiments that demonstrate the surface sensitivity of SHG and the effectiveness and versatility of SHG as a surface probe.

II. THEORETICAL BASIS

The general theory of surface SHG was developed earlier in 1962 by Bloembergen and Pershan.[17] Here, for simplicity, we consider only the case of an interface between a medium and vacuum. Recognizing that the properties of the interfacial region are different from those of the bulk, we can treat the problem as SHG from a three-layer system schematically shown in Fig. 1.[10] The thickness of the interfacial layer d is necessarily of microscopic dimension. Therefore, the nonlinear polarization $P^{(2)}(2\omega)$ which is responsible for the SHG can be written as

$$\vec{P}^{(2)}(2\omega) = 0 \qquad \text{for } z < 0$$

$$= \vec{P}_S^{(2)}\delta(z) + \vec{P}_B^{(2)} \qquad \text{for } z > 0 \qquad (1)$$

where

$$\vec{P}_S^{(2)} = \overleftrightarrow{\chi}_S^{(2)} : \vec{E}(\omega)\vec{E}(\omega)$$

$$\vec{P}_B^{(2)} = \overleftrightarrow{\chi}_B^{(2)} : \vec{E}(\omega)\vec{E}(\omega) \quad \text{for a medium without inversion symmetry}$$

$$= \overleftrightarrow{\chi}_{NL}^{(2)} : \vec{E}(\omega)\nabla\vec{E}(\omega) \quad \text{for a medium with inversion symmetry}$$

$$\vec{E}(\omega) = \vec{\mathcal{E}}\exp(i\vec{k}\cdot\vec{r} - i\omega t).$$

The SHG is then described by the solution of the Maxwell equations with $\vec{P}^{(2)}(2\omega)$ acting as the radiation source. For the reflected SH output,

or the homogeneous part of the transmitted SH output, it can be shown that the solution remains unchanged if $\vec{P}^{(2)}(2\omega)$ in Eq. (1) is replaced by an effective surface nonlienar polarization[18] such that

$$\vec{P}^{(2)}(2\omega) = 0 \qquad \text{for } z < 0$$

$$= \vec{P}^{(2)}_{S,eff}\delta(z) \qquad \text{for } z > 0 \tag{2}$$

where

$$(P^{(2)}_{S,eff})_j = P^{(2)}_{S,j} + iP^{(2)}_{B,j}/(k_{2,z} + k_{s,z}) \qquad \text{for } j = x,y,z$$

$$\vec{k}_s = 2\vec{k}(\omega)$$

and $\vec{k}_1$ and $\vec{k}_2$ are wavevectors of the free waves at 2ω reflected into the vacuum and trasmitted into the medium, respectively. The solution yields, for the $\hat{s}$- and $\hat{p}$-polarized SH wave radiated back into the vacuum,

$$E_s(2\omega) = \frac{i4\pi k_1^2}{k_{1,z} + k_{2,z}} (P_{S,eff})_y$$

$$E_p(2\omega) = \frac{i4\pi k_1}{\varepsilon k_{1,z} + k_{2,z}} [k_{2,z}(P_{S,eff})_x + k_{2,x}(P_{S,eff})_z]. \tag{3}$$

The output SH power is given by

$$\mathcal{P}(2\omega) = \frac{c}{2\pi} \int |\vec{E}(2\omega)|^2 dA. \tag{4}$$

Since the boundary condition requires $k_{1,x} = k_{2,x} = k_{s,x} = 2k_x(\omega)$, the output is expected to be highly collimated in a well defined direction.

Equation (1) shows that in order for SHG to be surface-specific, we must have $|P_S^{(2)}| \gtrsim (1/2k_2)|P_B^{(2)}|$. This would mean $|\chi_S^{(2)}| \gtrsim (1/2k_2)|\chi_B^{(2)}|$ or $|\chi_S^{(2)}|/|\chi_B^{(2)}|d \gtrsim 1/2k_2d$ if the medium has no inversion symmetry. Such an inequality is unlikely to hold since $k_2d << 1$. Therefore, SHG is generally not applicable to surface studies of a medium without inversion symmetry. If, however, the medium is centrosymmetric, then $\vec{P}_B^{(2)} = \overleftrightarrow{\chi}_{NL}^{(2)}:\vec{E}\vec{V}\vec{E}$ derived from electric quadrupole and magnetic-dipole contributions is ka times weaker than $\overleftrightarrow{\chi}_B^{(2)}:\vec{E}\vec{E}$ from the electric-dipole contribution, where a is the lattice constant or the size of the atoms or molecules in the medium. The condition $|P_S^{(2)}| \gtrsim (1/2k_2)|P_B^{(2)}|$ then becomes $|\chi_S^{(2)}|/|\chi_B^{(2)}|d \gtrsim a/d$ which, with $a \lesssim d$, can be satsified in many cases. This happens, for example, with metal surfaces where free electrons give rise to large surface nonlinearities, with semiconductor surfaces where dangling bonds with lone-pair electrons yield large surface nonlinearities, and with surface layers of molecular adsorbates that possess large nonlinearities. As we shall discuss later, the surface layer can dominate over the bulk in SHG in some cases; in other cases, the surface nonlinearity can be determined separately by appropriate measurements.

As an order-of-magnitude estimate, we can assume $|\chi_S^{(2)}|d \sim |\chi_B^{(2)}|$, which is normally in the 10^{-6}-10^{-8} esu range. With $d \sim 10^{-7}$ cm, we have, for a surface monolayer of atoms or molecules, $|\chi_S^{(2)}| \sim 10^{-13}$-$10^{-15}$ esu. One can also use the second-order perturbation calculation to give a rough estimate of $|\chi_S^{(2)}|$. Assuming the absence of local-field cor-

rection, and assuming the laser excitation far off resonance, we have

$$|\chi_S^{(2)}| \sim N_S \frac{\langle (er)^3 \rangle}{(\hbar\bar{\omega}_o)^2}. \tag{5}$$

With $N_S \sim 10^{14}$-$10^{15}/cm^2$ for a molecular monolayer, $r \sim 1$ Å, and $\bar{\omega}_o \sim 3 \times 10^{15}/sec$, we find $|\chi_S^{(2)}| \sim 10^{-14}$-$10^{-15}$ esu. Resonant enhancement can of course greatly enhance the value of $|\chi_S^{(2)}|$.

Knowing the value of $|\chi_S^{(2)}|$, we can estimate the signal strength of SHG from a surface layer. Equation (3) leads to a SH output[12]

$$S(2\omega) = 32\pi^2\omega^2 c^{-3} \sec^2\theta |\chi_S^{(2)}|^2 I^2(\omega) AT \tag{6}$$

for an input laser pulse with intensity $I(\omega)$, cross-section A, pulse duration T, and incidence angle θ. If we take $|\chi_S^{(2)}| \sim 10^{-15}$ esu, $I(\omega) \sim 10$ MW/cm^2, $A \sim 0.2$ cm^2, $T \sim 10$ nsec, and $\theta \sim 45°$, the signal strength S is of the order of 10^4 photons/pulse. Such a large signal should be readily detectable. This then predicts the submonolayer sensitivity of surface SHG. Measurement of the surface SHG allows us to deduce $\overleftrightarrow{\chi}_S^{(2)}$ for the surface layer.

From the surface science point of view, it is of course most important that the macroscopic $\overleftrightarrow{\chi}_S^{(2)}$ can be related to the surface properties. Unfortunately, the detailed microscopic understanding of $\overleftrightarrow{\chi}_S^{(2)}$ is still lacking. We can offer here only the following general picture. For a molecular monolayer adsorbed on a surface, the surface nonlinear susceptibility can be written as

$$\overleftrightarrow{\chi}_S^{(2)} = \overleftrightarrow{\chi}_{SS}^{(2)} + \overleftrightarrow{\chi}_M^{(2)} + \overleftrightarrow{\chi}_I^{(2)}. \qquad (7)$$

Here, $\overleftrightarrow{\chi}_{SS}^{(2)}$ is the contribution from the bare substrate surface, $\overleftrightarrow{\chi}_M^{(2)}$ is the contribution from the molecular layer isolated from the substrate, and $\overleftrightarrow{\chi}_I^{(2)}$ arises from interaction between the molecule and the substrate that changes the properties of both the molecule and the surface of the substrate. Whether a particular term dominates in Eq. (7) or not depends on the material system. In some cases, asymmetric molecules with large second-order nonlinear polarizabilities can yield a dominating $\overleftrightarrow{\chi}_M^{(2)}$ if they are aligned on the surface. In other cases, $\overleftrightarrow{\chi}_M^{(2)}$ may be negligible and the only effect of the adsorbates on $\overleftrightarrow{\chi}_S^{(2)}$ is a modification of $\overleftrightarrow{\chi}_{SS}^{(2)}$ by $\overleftrightarrow{\chi}_I^{(2)}$. While it is possible to make a reasonable guess at the physical origins of the various terms in Eq. (7) for a given surface system, a more quantitative picture would require a rather thorough understanding of the microscopic properties of the surface system. It is possible, for example, to use the bond theory to calculate $\overleftrightarrow{\chi}_S^{(2)}$ for semiconductor and insulator surfaces, but one needs prior knowledge of the surface structure.

The possible local-field effect on $\overleftrightarrow{\chi}_S^{(2)}$ is also a problem of great importance for understanding surface nonlinearity.[19] In the present case, the local-field correction arising from induced dipole-induced dipole interaction between molecules comes in two ways. First, the average local field leads to the usual expression between macroscopic and microscopic susceptibilities

$$\overleftrightarrow{\chi}_S^{(2)}(2\omega) = \overleftrightarrow{L}^{\dagger}(2\omega) \cdot \overleftrightarrow{\chi}_S^{(2)} : \overleftrightarrow{L}(\omega)\overleftrightarrow{L}(\omega)$$

where $\overleftrightarrow{L}$ is the local-field correction factor which is necessarily different from that for the bulk, and $\overleftrightarrow{\chi}_S^{(2)}$ is the microscopic susceptibility. Then, the strong spatial variation of the local field at the surface can modify the transition matrix elements and hence $\overleftrightarrow{\chi}_S^{(2)}$. The harmonic frequency component of the local field may also contribute, but it is believed to be less important. In the absence of any reasonable quantum theory of the local field, the classical point-dipole model is often used to calculate the local-field effect. For a surface layer of moleclar adsorbates, it has been found that the local-field correction (with respect to the incoming field in vacuum) is negligible if the nearest-neighbor distance between adsorbed molecules is more than ~ 10 Å and the distance between the molecules and the substrate is more than 2.5 Å in the metal case or more than 1.5 Å in the insulator case.

Aside from the above microscopic local-field correction, there also exists a macroscopic local-field correction (with respect to the incoming field) arising from the macroscopic boundary effect.[20] In the plane boundary case, for example, the macroscopic local-field correction is simply described by the Fresnel factor for transmission. On a rough metal surface with structure of the order of a wavelength in size, this local-field correction can be very large, leading to a local-field enhancement of surface SHG several orders of magnitude stronger than that from a smooth surface.

III. STUDY OF SURFACE ENHANCEMENT OF OPTICAL PROCESSES BY SECOND HARMONIC GENERATION

It was discovered some time ago that the effective Raman cross-section of molecules can increase by many orders of magnitude when adsorbed on roughened noble metal surfaces.[21] The cause of this large surface enhancement and the promise that surface-enhanced Raman scattering (SERS) may be useful as a sensitive tool for surface spectroscopy have attracted a great deal of attention. Two general mechanisms contribute to the enhancement. First, a chemical interaction between the adsorbed molecules and the substrate can lead to a larger intrinsic Raman cross-section than that of an isolated molecule. Second, the incoming and outgoing optical fields can be enhanced by the macroscopic local-field enhancement mentioned earlier. For metals, the local-field enhancement on a rough surface could be exceptionally strong because of the presence of local plasmon resonances and corona (or lightning rod) effects in the local structures. In Raman scattering, these two mechanisms are both present, and it is difficult to distinguish one from the other. Moreover, unless the surface enhancement is larger than $\sim 10^3$, the SERS signal is not easy to detect. This limits the possibility of SERS measurements to only a few metals, namely, the noble metals.

We realize, however, that Raman scattering, being a two-photon transition, is a nonlinear optical effect, and any nonlinear optical process should experience a surface local-field enhancement. If we are interested in exploring only the surface local-field enhancement, it is more appropriate to study those optical effects that can be observed on bare metal surfaces. Without adsorbates (or with the same adsorbates on

both smooth and rough surfaces), surface enhancement due to chemical interaction does not come into play. Comparison of the signal strength from rough and smooth surfaces will then yield the local-field enhancement alone. Surface SHG is ideal for such study not only because the experiment is relatively simple, but also because it provides easily detectable signals from both smooth and rough surfaces of any metal.[20,22]

In terms of the macroscopic local-field correction factor $\mathscr{L}$, the effective nonlinear susceptibility for surface SHG is given by

$$(\chi_S^{(2)})_{eff} = \mathscr{L}(2\omega)\chi_S^{(2)}\mathscr{L}(\omega)\mathscr{L}(\omega) \tag{8}$$

and the surface enhancement is expected to be

$$\eta_{SH} \propto \frac{1}{A}\int \mathscr{L}^2(2\omega)\mathscr{L}^4(\omega)dA \tag{9}$$

where the integration is over the rough surface structure. On some local tips, $\mathscr{L}(\omega)$ is a maximum because of local plasmon resonance, but then $\mathscr{L}(2\omega)$ is likely to be close to unity. If $\mathscr{L}^4_{max}(\omega)$ dominates in the above integral, then Eq. (9) can be approximated by

$$\eta_{SH} \propto f\mathscr{L}^4_{max}(\omega) \tag{10}$$

with f being the fractional area where $\mathscr{L}_{max}(\omega)$ occurs. For Raman scattering, the Raman cross-section σ_R is directly proportional to the imaginary part of $\chi^{(3)}(\omega_s = \omega_\ell - \omega_\ell + \omega_s)$. The surface local-field enhancement of σ_R is easily shown to be

$$\eta_R \propto \frac{1}{A} \int \mathscr{L}^2(\omega_\ell)\, \mathscr{L}^2(\omega_s)\, dA. \qquad (11)$$

If $\omega_\ell \sim \omega_s \sim \omega$, and $\mathscr{L}^4_{max}(\omega)$ dominates in the integral, we again have

$$\eta_R \propto f\, \mathscr{L}^4_{max}(\omega). \qquad (12)$$

Thus, measurement of the local-field enhancement of surface SHG should also allow us to determine the local-field enhancement in SERS.

The experimental arrangement for surface SHG is shown in Fig. 2. While the SH output from a smooth surface is highly directional, the one from a rough surface is highly diffusive because of roughness scattering. The surface enhancement was measured by comparing the total diffuse SH output from the rough surface to the coherent SH output from the smooth surface. Indeed, as shown in Fig. 3, we found, with a pump beam at 1.06 μm, a surface enhancement of $\sim 10^4$ on an electrochemically roughened surface. This would correspond to a local-field enhancement of $\sim 10^6$ in SERS with respect to Raman scattering from isolated molecules. With the pump field at 0.683 μm, the measured local-field enhancement in surface SHG was 10^2. This should correspond to a local-field enhancement of $\sim 10^5$ in SERS. The dielectric dispersion is expected to reduce the enhancement of SERS at 0.54 μm to 2×10^4. The measured surface enhancement of SERS at 0.54 μm, including both the local-field and the chemical effects, was $\sim 10^6$. We can therefore conclude that an enhancement of ~ 50 may arise from the pyridine-Ag interaction.

The observation of surface-enhanced SHG on rough Ag surfaces clearly demonstrates the importance of local-field enhancement on surface non-

linear optical processes. The high sensitivity of surface SHG now allows us to measure not only the surface enhancement on noble metals but also that on other metals or solids. This has recently been carried out with samples of identical roughness so that the relative enhancement can be deduced.[22] Among the 16 metals studied, Ga, Mg, and Aℓ appeared to have a local-field enhancement comparable to or larger than Ag. The results suggest that SERS may be possible on quite a few different metal surfaces, considering that the chemical interaction between molecules and substrates should further enhance the Raman effect.

IV. STUDY OF MOLECULAR ADSORPTION AND DESORPTION ON ELECTRODES IN AN ELECTROLYTICAL CELL

Electrochemistry is a very old discipline, but the understanding of electrochemistry is still at a very primitive stage. One of the major difficulties is that very little is known about adsorbates on electrodes.

We showed in Sec. II that surface SHG has the sensitivity of detecting a submonolayer of molecular adsorbates. On a roughened metal electrode, the surface enhancement could further improve the detection sensitivity. It is therefore possible to use surface SHG to study molecular adsorption and desorption at an electrode.[12] An example is shown in Fig. 4, where surface SHG from a Ag electrode in a 0.1 M KCℓ solution is found to respond to the appearance and disappearance of AgCℓ on the electrode. The signal increases rapidly when the first monolayer of AgCℓ is formed at the roughened electrode, as judged from the amount of charge transfer through the electrode, and decreases precipitately when the last monolayer of AgCℓ is reduced back to Ag and Cℓ. In between,

although hundred of AgCl monolayers are formed and reduced, the signal varies only slightly, mostly in response to the change in surface roughness. This is the result of the surface-specific nature of SHG. If 0.05 M of pyridine is added into the solution and a sufficiently negative bias is put on the Ag electrode, it is known that pyridine molecules would adsorb to the Ag surface at some active sites with no more than a monolayer. Yet the surface SHG signal is Fig. 4 shows that it can clearly respond to the adsorption of pyridine.[12] When a laser pulse of 0.2 mJ of energy at 1.06 μm and 6 nsec in pulsewidth was focused to a spot of 0.2 cm^2 on the pyridine-adsorbed electrode, a signal level of 8 $\times 10^5$ photons/pulse was detected. Knowing that the enhancement of SHG on such a surface is $\sim 10^4$, and assuming that the surface coverage of pyridine is $4 \times 10^{14}/cm^2$, we can deduce from Eq. (6) a value of the nonlinear susceptibility per adsorbed pyridine molecule to be -8×10^{-30} esu.

Unless a tunable laser is used, the SHG technique is not spectrally selective. This is certainly a disadvantage of the technique. Another difficulty is the lack of microscopic understanding of the surface nonlinearity incurred by the adsorbates. For example, it is not understood why the SHG signal increases when pyridine molecules are adsorbed on the Ag electrode in the electrolytical solution[12] while it decreases when the same molecules are adsorbed on Rh(111) in an ultrahigh vacuum.[16] The dc-field-induced SHG was not important in the case of Ref. 12, as judged from the signal dependence on the bias voltage. It may happen that the adsorption of pyridine on Ag induces a charge-transfer band in the green at which the SHG is resonantly enhanced.

The possible applications of SHG to electrochemistry are yet to be explored. As long as the adsorbed species on an electrode can be identified by some means (for example, SERS), surface SHG can be used to study the time dependence of adsorption or desorption of that species, and to help monitor molecular adsorption and desorption during an electrolytic cycle.[20,23] In another case, when a fixed number of adsorbates exist on an electrode, the surface SHG as a function of the bias voltage allows us to find the effective surface charge density on the electrode.[24]

V. STUDY OF MOLECULAR ADSORBATES ON INSULATORS

While rough surfaces may be of practical importance in surface science, smooth surfaces are obviously better characterized and easier to analyze. We discuss here applications of surface SHG to the study of molecular adsorbates at gas/solid and liquid/solid interfaces. As we showed earlier, surface SHG has the sensitivity to detect a molecular submonolayer, and can therefore be used to study molecular adsorbates. We shall describe in the following how information about the spectrum, the symmetry of molecular arrangement, the average molecular orientation, and the adsorption isotherm of the adsorbates can be deduced from the SHG measurements.[13,14] In all the examples given, smooth fused quartz plates were used as the substrates. They generally give much weaker SH signals than the adsorbates.

A. Spectroscopic Study of Molecular Adsorbates

SHG from an adsorbed molecular layer should be resonantly enhanced when either the fundamental or the second harmonic frequency coincides with an absorption band of the molecules. Thus, surface SHG with a tun-

able laser can yield a resonant spectrum of the molecular adsorbates. We use here dye molecules adsorbed at an air/fused quartz interface as an example.[13]

The sample was prepared by depositing half monolayer of dye molecules on a quartz plate using either the spinning or the dipping technique. The experimental setup in Fig. 2 was then used to measure the SHG from the dye molecular layer. The resonant structure in SHG versus the laser frequency was expected to reflect the resonant transitions in the dye molecules. This is illustrated by the examples of Rhodamine 6G and Rhodamine 110 dyes in Fig. 5, where scanning of 2ω over the $S_0 \rightarrow S_2$ electronic transition of the molecules yields the observed resonant peaks. Because of the slight difference in their molecular structures, the resonant peaks of the two dye molecules are shifted slightly from each other. The signal rise towards the low-frequency side indicates the appearance of another resonant peak as ω approaches the $S_0 \rightarrow S_1$ transition.

The SH signal from dye molecules was very strong. With a pump laser energy of 1 mJ in a pulsewidth of 5 nsec focused to a spot of 10^{-3} cm^2, the observed signal from a half monolayer of Rhodamine 6G ($N \sim 5 \times 10^{13}$/cm^2) was $\sim 10^4$ photons/pulse on resonance, corresponding to a nonlinear susceptibility $\chi^{(2)} \sim 7 \times 10^{-29}$ esu/molecule. Such a large nonlinear susceptibility was the combined effort of the resonance of 2ω with the $S_0 \rightarrow S_2$ transition, the near resonance of ω with the $S_0 \rightarrow S_1$ transition, and the large dipole moments of the transitions involved. In fact, in one type of coumarine dye molecules, one can find both ω and 2ω simultaneously resonant with the $S_0 \rightarrow S_1$ and $S_0 \rightarrow S_2$ transitions, respective-

ly. As a result, the SH signal from such molecules is - 10^3 times larger than that from Rhodamine 6G.[25]

The discussion here shows that surface SHG can be used to do spectroscopy on adsorbed molecules. The method is, of course, not limited to adsorbates on insulator surfaces. One can use it, for example, to study the charge-transfer band created by adsorption of molecules on metals. So far, with tunable dye lasers, only the electronic transitions of adsorbates can be probed. In surface science, vibrational spectroscopy of adsorbates is of tantamount importance since the spectra allow one to deduce the molecule-substrate interaction.[26] One would think that this could be achieved by surface SHG using a tunable infrared laser. However, infrared detectors are generally much less sensitive than photomultipliers in the visible, so that infrared SHG is not likely to have the necessary sensitivity to study submonolayer adsorbates. It is, however, possible to use yet another second-order process, sum-frequency generation, instead of SHG for vibrational spectroscopy. In this case, a tunable infrared laser is used to probe the vibrational transitions of the adsorbates, and the resonant spectrum can be up-converted to the visible by sum-frequency generation using a visible laser. A preliminary experiment shows that this is indeed a viable method.[27]

B. Probing of Symmetry of Molecular Arrangement

SHG generated from a layer of adsorbates could be used to probe the symmetry of the molecular arrangement in that layer. This is based on the idea that the structural symmetry may be reflected by the azimuthal variation of SHG as the sample rotates about its surface normal. Simple calculation can show that a molecular arrangement with C_4 or higher rota-

tional symmetry should yield an SH signal with isotropic azimuthal variation, but those with lower symmetry should give rise to a corresponding rotational symmetry in the azimuthal variation of the SH signal.

The above discussion actually assumes that the adsorbed molecules are correlated by chemical or/and electromagnetic interaction. Otherwise, we would have the surface nonlinear susceptibility given by $\overleftrightarrow{\chi}_S^{(2)} = N_S\langle\overleftrightarrow{\alpha}\rangle^{(2)}$ with $\langle\overleftrightarrow{\alpha}\rangle^{(2)}$ being the average nonlinear polarizability of individual adsorbed molecules and N_S the surface density of the adsorbates. The symmetry of $\overleftrightarrow{\chi}_S^{(2)}$ which is exhibited by the symmetry in SHG would then reflect only the symmetry of $\langle\overleftrightarrow{\alpha}\rangle^{(2)}$ for individual molecules instead of that for the molecular arrangement.

Measurements of SHG as a function of rotation about the surface normal have been carried out for dye molecules and p-nitrobenzoic acid molecules adsorbed on fused quartz.[13,14] In these cases, the signal was found to be independent of the rotation. This suggested several possibilities: (1) molecules were randomly distributed, and also randomly oriented with respect to the azimuthal angle ϕ; (2) molecules formed a surface lattice, but they were uncorrelated and randomly oriented with respect to ϕ; (3) correlated molecules formed a surface lattice with C_4 or higher rotational symmetry, but they were randomly oriented with respect to ϕ. We believe that the first possibility is most likely, since on an amorphous substrate, molecules would form a lattice only through correlation, and then, correlation should also forbid a random orientation of the molecules with respect to ϕ.

In general, if the molecular adsorbates do form a surface lattice, we expect that their orientations are also well defined. It is then

possible that through the SHG measurement with the sample rotating about its surface normal and with different combinations of beam polarizations, we can obtain information both on the symmetry of the lattice and on the molecular orientation. Thus, we have a means to study, for example, how the molecular orientation varies as a two-dimensional molecular layer changes from a liquid to a solid phase.

C. Probing of Molecular Orientations of Adsorbates

Surface SHG with various polarization combinations can be used to deduce information about orientations of molecular adsorbates in some cases.[14] The basic underlying principle is fairly simple. The macroscopic nonlinear susceptibility is related to the microscopic nonlinear polarizability of the molecules by a coordinate transformation which depends on the molecular orientation. In the simple case where interaction between molecules is negligible, we have

$$(\chi_S^{(2)})_{ijk} = \sum_\lambda [G_{ijk}^{\xi\eta\zeta}(\theta,\phi,\psi)]_\lambda \alpha_{\xi\eta\zeta}^{(2)}$$

$$= \langle G_{ijk}^{\xi\eta\zeta}(\theta,\phi,\psi)\rangle N_S \alpha_{\xi\eta\zeta}^{(2)}. \qquad (13)$$

Here, $G_{ijk}^{\xi\eta\zeta}$ is the geometric factor specified by the transformation from the molecular coordinates (ξ,η,ζ) to the lab coordinates (i,j,k), θ, ϕ, ψ are the Euler angles describing the molecular orientation, the subindex λ denotes the different molecules, and the angular brackets indicate an average over all the molecules. It is seen from Eq. (13) that if $\alpha_{\xi\eta\zeta}^{(2)}$'s are known and $\chi_{ijk}^{(2)}$'s can be measured, then $\langle G_{ijk}^{\xi\eta\zeta}(\theta,\phi,\psi)\rangle$ can be obtained, from which a weighted average orientation of the molecules

can be deduced. Unfortunately, for a given molecular species, only very limited information about $\alpha^{(2)}_{\xi\eta\zeta}$ is usually available. Thus, only in special cases can we use the technique to really measure the orientation of adsorbates. This happens, for example, when $\alpha^{(2)}_{\xi\xi\xi}$ along a certain direction ξ dominates over all the other elements of $\overleftrightarrow{\alpha}^{(2)}$.

We consider here the orientational measurement on p-nitrobenzoic acid (PNBA) molecules adsorbed on fused quartz.[14] It is known that PNBA is adsorbed with the CO_2 end attached to the quartz surface, as shown in Fig. 6. The nonlinear polarizability $\overleftrightarrow{\alpha}^{(2)}$ of PNBA in this case is not expected to be much affected by the adsorption. The C_{2v} symmetry of PNBA leads to the following nonvanishing elements of $\overleftrightarrow{\alpha}^{(2)}$: $\alpha^{(2)}_{z'z'z'}$, $\alpha^{(2)}_{z'x'x'}$, $\alpha^{(2)}_{z'y'y'}$, $\alpha^{(2)}_{x'z'x'} = \alpha^{(2)}_{x'x'z'}$, $\alpha^{(2)}_{y'z'y'} = \alpha^{(2)}_{y'y'z'}$, where $\hat{x}' - \hat{z}'$ describes the molecular plane with $\hat{z}'$ along the long molecular axis, and $\hat{y}'$ is normal to the molecular plane. For molecules like PNBA having delocalized electrons around the ring, transition dipole moments perpendicular to the molecular plane are generally much smaller than the in-plane moments. Also, the transition moments along $\hat{x}'$ are generally smaller than those along $\hat{z}'$. Theoretical calculations show that $\alpha^{(2)}_{z'z'z'}$ is one order of magnitude larger than $\alpha^{(2)}_{x'z'x'}$ and $\alpha^{(2)}_{z'x'x'}$, and is three orders of magnitude larger than $\alpha^{(2)}_{y'z'y'}$ and $\alpha^{(2)}_{z'y'y'}$.[28] In the first-order approximation, therefore, we can assume $\alpha^{(2)}_{z'z'z'}$ to be the only nonvanishing element. Under this approximation, the PNBA molecule is treated as a long rod along $\hat{z}'$, and we like to find the orientation of this rod from the polarization dependence of SHG.

In the experiment, the observed SHG from adsorbed PNBA was independent of the sample rotation about the surface normal.[14] This indicated

that the molecules were randomly oriented with respect to the azimuthal angle ϕ. We only had to measure the angle θ between the molecular axis $\hat{z}'$ and the surface normal $\hat{z}$. For an isotropic surface layer, the non-vanishing elements of $\overleftrightarrow{\chi}_S^{(2)}$ are $\chi_{S,zzz}^{(2)}$, $\chi_{S,zxx}^{(2)} = \chi_{S,zyy}^{(2)}$, and $\chi_{S,xzx}^{(2)} = \chi_{S,yzy}^{(2)}$, and the relations between $\overleftrightarrow{\chi}_S^{(2)}$ and $\overleftrightarrow{\alpha}^{(2)}$ in the absence of intermolecular interaction are

$$\chi_{S,zzz}^{(2)} = N_S\langle\cos^3\theta\rangle\alpha_{z'z'z'}^{(2)}$$

$$\chi_{S,zxx}^{(2)} = 1/2\ N_S\langle\cos\theta\ \sin^2\theta\rangle\alpha_{z'z'z'}^{(2)}$$

$$\chi_{S,xzx}^{(2)} = 1/2\ N_S\langle\cos\theta\ \sin^2\theta\rangle\alpha_{z'z'z'}^{(2)}. \qquad (14)$$

The above equations then show that measurement of the ratio of $\chi_{S,zzz}^{(2)}$ to $\chi_{S,zxx}^{(2)}$ or the ratio of their linear combinations can yield a weighted average of θ.

Experimentally, the following ratio

$$R = [\chi_{S,zzz}^{(2)} + 2\chi_{S,zxx}^{(2)}]/\chi_{S,xzx}^{(2)}$$

$$= \langle\cos\theta\rangle/\langle\cos\theta\ \sin^2\theta\rangle \qquad (15)$$

can be easily measured by a polarization null method.[14] The value of R obtained by a 0.532 μm laser excitation for 1/4 monolayer of PNBA (N_S = $1.5 \times 10^{14}/cm^2$) adsorbed at an air/fused quartz interface was 2.3. To find the average orientation angle, we must know the orientational dis-

tribution. This information is unfortunately difficult to obtain. If we assume all molecules had the same θ, then from Eq. (15), we would have $\theta = 70°$. If we assume a Lorentzian distribution with a 10° FWHM spread, then the center of the distribution would lie at 76°. The same measurement carried out with 1/2 monolayer of PNBA at an ethanol liquid/fused quartz interface gave $R = 5.5$, which yielded $\theta = 36°$ for a δ-function distribution or $\theta = 34°$ at the center of a 10° Lorentzian distribution. The difference in the orientations of PNBA molecules at air/quartz and ethanol/quartz interfaces is easily understood from the interaction of the molecules with their surroundings. The interaction between PNBA and the silica would favor a flat orientation of the molecules on the substrate, but in ethanol, the dielectric effect of the solution and the interaction between the NO_2 group of PNBA and ethanol would like to tilt the molecules more towards the normal.

To check the validity of the technique, we note that the orientation of molecules is certainly independent of the laser frequency we use to do the measurements. Therefore, if measurements with different laser frequencies yield the same orientation angle, the result should be reliable. Indeed, at three different laser wavelengths 1.06, 0.683, and 0.532 μm, we found, assuming a δ-function distribution, $\theta = 38°$, 43°, and 37° (± 3°), respectively. The result here also indicates that the local-field effect on the determination of orientations is not significant. If the local-field correction is important, Eq. (14) will have to be replaced by

$$\chi^{(2)}_{S,zzz} = N_S \langle \cos^3\theta \rangle L_\perp(2\omega) L_\perp^2(\omega) \alpha^{(2)}_{z'z'z'},$$

$$\chi^{(2)}_{S,zxx} = 1/2\ N_S\langle\cos\theta\ \sin^2\theta\rangle L_\perp(2\omega)L_\parallel^2(\omega)\alpha^{(2)}_{z'z'z'}$$

$$\chi^{(2)}_{S,xzx} = 1/2\ N_S\langle\cos\theta\ \sin^2\theta\rangle L_\parallel(2\omega)L_\perp(\omega)L_\parallel(\omega)\alpha^{(2)}_{z'z'z'} \qquad (16)$$

where $L_\perp$ and $L_\parallel$ are the local-field correction factors for fields normal and parallel to the surface plane, respectively. The ratio R define in Eq. (15) will then depend on the L's. Because the local field is a function of frequency, R must also vary with frequency. This is particularly true if the frequency scans over resonances. In the above-mentioned experiment, the second harmonic of the 0.532-μm laser excitation was resonant with the $A_1 \rightarrow A_1$ transition of the PNBA molecules, while that of the 1.06 μm excitation was not. The fact that the measured R and the deduced orientation angle θ did not seem to have significant dependence on the laser frequency was therefore an indication that the local-field effect was not important. The result here is actually supported by a theoretical estimate of the local-field correction based on a point-dipole model,[19] which shows $L_\parallel \sim 1$ and $L_\perp \sim [1 + (1/4)\cos^2\theta]^{-1}$ at $N_S = 2 \times 10^{14}/cm^2$.

If the adsorbed molecules cannot be treated as rod-like, the determination of molecular orientation becomes much more complicated. The case of rhodamine dye molecules on fused quartz is an example.[13] The fact that SHG from the adsorbed layer was observed readily indicates that the molecules are not likely to lie flat on the substrate. However, to find the orientation of the molecular plane, we must refer to two possible models, one with the two amino groups attached to the sur-

face and the other with the acid group and one of the amino groups bound to the surface. The polarization measurement of SHG was only consistent with the latter model and suggested that the molecular plane was canted at 34° away from the surface normal. That adsorbed dye molecules are canted with the acid (carboxyphenil) group responsible for adsorption has also been confirmed by the orientation measurements on a group of selected xanthene dyes.[29]

D. Measurement of an Adsorption Isotherm for Adsorbates at a Liquid/Solid Interface

The adsorption isotherm for molecular adsorption at a liquid/solid interface is defined as the surface density of the adsorbates as a function of the adsorbate concentration in liquid. It is most useful for describing the characteristics of adsorption in equilibrium. One would therefore like to be able to measure directly such an isotherm. This can be achieved by surface SHG if the local-field correction is negligible.

Without the local-field correction, the SH field generated by the N_S adsorbed molecules/cm^2 is proportional to $\chi_S^{(2)} = N_S\langle\alpha^{(2)}\rangle$. By measuring the SH output as a function of the adsorbate concentration ρ, we should then be able to deduce the adsorption isotherm N_S versus ρ. In practice, however, SHG from the bulk liquid and solid constituting the interface may not be negligible, especially when N_S is small. The observed SH signal should then very with N_S as

$$S = |A + BN_S|^2 \qquad (17)$$

where the A and B parts refer to contributions from the background and the adsorbed molecules, respectively. We then have

$$N_S = \left|\frac{A}{B}\right|\{[\frac{S}{|A|^2} - 1 + \cos^2\phi]^{1/2} - \cos\phi\} \qquad (18)$$

with $B/A = |B/A|\exp(i\phi)$. Since $|A|^2$ and ϕ can be separately determined, the measured signal S allows us to deduce N_S; the proportional constant $|A/B|$ in Eq. (18) can be calibrated against the saturated surface density. In this scheme, we have also implicitly assumed that the orientation of the adsorbates does not very with surface density. If not, further correction must be made.

We present in Fig. 7 the isotherm of PNBA adsorption from ethanolic solution to fused quartz measured by the above technique using a 0.532-μm laser excitation.[14] Within the experimental accuracy, the orientation of PNBA appeared to be independent of ρ. The isotherm has the general shape associated with Langmuir kinetics, increasing monotonically without kinks to a saturation level. As we expect, the low concentration region more closely obeys the Langmuir equation

$$N_S/N_0 = \rho/(\kappa + \rho) \qquad (19)$$

which is based on the assumption that the adsorption of molecules to

empty sites is independent of the molecules already present on the surface. Here, N_0 is the saturation surface density and $\kappa = 55\exp(-\Delta G/RT)$ with ΔG being the free energy of adsorption, R the gas constant, and T the temperature. Fitting the first few data points in Fig. 7 to Eq. (19) yields $\Delta G = 8$ KCal/mole for the adsorption of PNBA from ethanol to fused quartz.

VI. STUDY OF SEMICONDUCTOR SURFACES

Since the surface specificity of SHG relies on the inversion symmetry of the bulk media, surface SHG as a surface tool is only applicable to the centrosymmetric semiconductors such as Si and Ge. As in the insulator case, we can use surface SHG to study molecular adsorption on the surfaces of such semiconductors. Moreover, the method is also applicable to the study of bare semiconductor surfaces. This is particularly interesting because of the possibility of using the technique to investigate surface annealing and surface reconstruction. However, although SHG is forbidden in the bulk, it is not strictly zero owing to the nonvanishing electric-quadrupole and magnetic-dipole contribution. To study surfaces by SHG, we must be able to distinguish the surface SHG signal against the background signal from the bulk. This is obviously more difficult than in the absorbate case where the background signal comes from the substrate and the surface coverage of absorbates is variable. By proper polarization arrangements, the anisotropic part of the surface and bulk contributions can actually be determined separately.[15]

A. Surface versus Bulk Contribution in SHG from Si Surfaces

We discuss here the measurements that allow us to compare surface

and bulk contributions to SHG, using Si as an example. As stated in Eq. (2), the effective nonlinear polarization for surface SHG consists of a surface term and a bulk term. For a cubic medium under the excitation of a single plane wave, the bulk nonlinear polarization has the form

$$P_{B,j}^{(2)} = \gamma\nabla_j[\vec{E}(\omega) \cdot \vec{E}(\omega)] + \zeta E_j(\omega)\nabla_j E_j(\omega) \tag{20}$$

where j's are taken along the [100] axes. In Eq. (20), γ describes the isotropic contribution and ζ the anisotropic contribution. The form of the surface nonlinear polarization $\vec{P}_S^{(2)} = \overleftrightarrow{\chi}_S^{(2)}:\vec{E}\vec{E}$ depends on the surface chosen. For the (100) surface, it is identical to that for the isotropic case with $\chi_{S,zzz}^{(2)}$, $\chi_{S,zxx}^{(2)} = \chi_{S,zyy}^{(2)}$, and $\chi_{S,xzx}^{(2)} = \chi_{S,yzy}^{(2)}$ being the only nonvanishing elements of $\overleftrightarrow{\chi}_S^{(2)}$. For the (111) surface, the 3m symmetry allows additional elements $\chi_{S,\xi\xi\xi}^{(2)} = -\chi_{S,\xi\eta\eta}^{(2)} = -\chi_{S,\eta\xi\eta}^{(2)}$ to contribute. Here, $\hat{\xi}$ is along the projection of a (100) axis on the surface and $\hat{\eta}$ is 90° from $\hat{\xi}$ in the surface plane. It can then be shown that the surface SH signal S has the following functional dependence on the angle of rotation of the sample about its surface normal

$$S = |A + Bf(\psi)|^2 \tag{21}$$

where ψ is the angle between the lab x-axis and a chosen [100] crystal axis in the surface or its projection on the surface.

The detailed expressions of S for the various surfaces can be obtained from Eqs. (3) and (6).[27] Their characteristic features, however,

can be easily derived from simple physical reasoning. (1) $f(\psi)$ should reflect the structural symmetry: it exhibits a 3-fold symmetry for the (111) surface and a 4-fold symmetry for the (100) surface. (2) A and B are constants depending on the surface chosen and the input and output beam polarizations and directions. A represents the isotropic contribution and is a linear combination of the isotropic elements of $\overleftrightarrow{\chi}^{(2)}_{S,eff}$ defined by $\vec{P}^{(2)}_{S,eff} = \overleftrightarrow{\chi}^{(2)}_{S,eff}:\vec{E}(\omega)\vec{E}(\omega)$, or more correctly, a linear combination of $\chi^{(2)}_{S,zzz} - \gamma$, $\chi^{(2)}_{S,zxx} - \gamma$, $\chi^{(2)}_{S,xzx}$, ζ, and $\chi^{(2)}_{S,\xi\xi\xi}$. The B term describes the anisotropic contribution, and therefore, the constant B is a linear combination of only the anisotropic susceptibility elements $\chi^{(2)}_{S,\xi\xi\xi}$ and ζ. (3) Since the (yxx), (yxz), (yzz) elements of the isotropic $\chi^{(2)}_{S,eff}$ are all zero, we have A = 0 if the laser input is p-polarized (in the $\hat{x}$-$\hat{z}$ plane) and the SH output is s-polarized. (4) For the (100) surface, $\chi^{(2)}_{S,\xi\xi\xi}$ does not contribute to S, and B depends only on ζ. From the above description, it can be seen that by using various combinations of input and output polarizations, one should be able to deduce from the measurements of SHG the nonlinear susceptibility elements $\chi^{(2)}_{S,zzz} - \gamma$, $\chi^{(2)}_{S,zxx} - \gamma$, $\chi^{(2)}_{S,xzx}$, ζ, and $\chi^{(2)}_{S,\xi\xi\xi}$. They are generally complex quantities; their phase factors can be determined separately by measuring the phases of the SH outputs.

The measurements have actually been carried out on silicon.[15] The samples were etched and polished by Syton, and exposed to air during the measurements. It was expected that a thin layer of silicon oxide might exist on the surfaces, but it should be amorphous and its nonlinearity small. Part of the experimental results of SHG as a function of ψ obtained by a 0.532 μm $\hat{p}$-polarized pump laser from the (111) surface are

shown in Fig. 8 as an example. In Fig. 8a, the SH output is s-polarized; hence, A = 0 in Eq. (21), and the 3-fold rotational symmetry reflected in $f(\psi)$ appears as a 6-fold symmetry in S. In Fig. 8b, the output is p-polarized. With a 45° incident angle, it happens that A = B in Eq. (21). Consequently, S exhibits a 3-fold symmetry with only three peaks. As seen in the figure, the experimental curve can be fit very well by theory, and therefore, the determination of the nonlinear susceptibility elements can be quite accurate. By measuring the $\hat{p}$-polarized and $\hat{s}$-polarized SH outputs for both $\hat{p}$- and $\hat{s}$-polarized inputs, and in addition, the $\hat{s}$-polarized output for an input with mixed polarization, we whould have sufficient measurements to determine all the five nonvanishing elements. The results are[27]

$$\chi^{(2)}_{S,zzz} - \gamma = 55\zeta' \exp(-i120°)$$

$$\chi^{(2)}_{S,zxx} - \gamma = 3.1\zeta' \exp(-i50°)$$

$$\chi^{(2)}_{S,xzx} = 5.1\zeta' \exp(-i148°)$$

$$\chi^{(2)}_{S,\xi\xi\xi} = 1.6\zeta' \exp(i22°)$$

where $\zeta' = [\omega/c(k_{2z} + k_{sz})]\zeta = 0.138\zeta \exp(-i35.6°)$ is the effective surface nonlinear susceptibility arising from the bulk nonlinear optical constant ζ.

The above result shows that $|\chi^{(2)}_{S,zxx} - \gamma| \sim |\chi^{(2)}_{S,xzx}|$. Since we expect from Kleinman's rule that $|\chi^{(2)}_{S,zxx}| \sim |\chi^{(2)}_{S,xzx}|$, we can con-

clude that γ is at most of the same order as $|\chi^{(2)}_{S,zxx}|$. Thus, we have for the surface nonlinear susceptibility elements, $|\chi^{(2)}_{S,zzz}| > |\chi^{(2)}_{S,zxx}|$, $|\chi^{(2)}_{S,xzx}| > |\chi^{(2)}_{S,\xi\xi\xi}|$. This can be understood from the fact that the surface layer has much higher asymmetry in the surface normal ($\hat{z}$) direction than in the surface plane. Although the anisotropic element $\chi^{(2)}_{S,\xi\xi\xi}$ is relatively small, it can still contribute as much as $\chi^{(2)}_{S,zzz}$ to the SH radiation. The higher efficiency of $\chi^{(2)}_{S,\xi\xi\xi}$ comes from the larger Fresnel factor for the fields parallel to the surface. In comparison with the bulk anisotropic contribution, the surface term also dominates because of the higher radiation efficiency even though $|\chi^{(2)}_{S,\xi\xi\xi}| \sim |\zeta'|$.

We should remark that the above experiment was carried out on sample surfaces exposed to air. Consequently, the surface layer should include an amorphous silicon oxide overlayer. However, a separate experiment had shown that SHG from fused silica is at least two orders of magnitude weaker than the one from a Si surface. Thus, the contribution of the silica overlayer to the overall SHG from Si should be negligible. The SiO_2/Si interface is certainly different from the vacuum/Si interface for a bare Si surface. As we shall see later, the oxide layer actually decreases the SH signal from Si.[30]

B. Probing Phase Transitions on Semiconductor Surfaces

We have seen that SHG as a function of sample rotation ϕ about the surface normal can reflect the structural symmetry of a sample. If the contribution from the surface layer dominates in the SHG, then the method can be used to probe the structure symmetry of the surface layer. Shank et al.[31] have actually employed the technique to study the dynamics

of laser-induced melting. A femptosecond laser pulse with sufficient energy for laser-induced melting was first impinged on a Si(111) surface. Another femptosecond pulse with adjustable time delay was then used to generate SH from the irradiated surface. When the surface was not yet melted, the SH signal exhibited a 3-fold symmetry with respect to ϕ. After the surface was melted, the SH signal became isotropic in ϕ. From such a measurement, they were able to conclude that it took ~ 1 psec for the Si(111) surface to melt when excited by a 90-fsec laser pulse of 0.2 mJ/cm^2 at 6200 . Using the same technique, Akhmanov et al. have investigated laser-induced melting of a GaAs surface.[32]

More recently, Heinz et al. have used SHG to probe the structural change of a bare Si surface.[33] A freshly cleaved Si(111) surface in vacuum is known to reconstruct to form a 2 × 1 structure as seen by low-energy electron diffraction (LEED). After annealing, it is expected to change to a 7 × 7 structure. The 2 × 1 structure should yield a 2-fold symmetry in the SHG as a function of ϕ, while the 7 × 7 structure should lead to an isotropic variation. This is indeed what was observed. The fact that SHG can distinguish different surface structures opens a new area of surface studies: Since SHG is a process with an instantaneous response, we can use it to study the dynamics of transition from one surface structure to another with a time resolution only limited by the laser pulsewidth.

C. Monitoring Adsorbates on a Semiconductor Surface

Atomic or molecular adsorption on Si and Ge can also be monitored by SHG. The sensitivity is quite high in the case of chemisorption. It is known that dangling bonds exist on clean Si and Ge surfaces. Because of

asymmetry, these bonds are highly nonlinear. As a result, SHG from bare Si or Ge is dominated by the surface contribution. When adsorption quenches the dangling bonds, the surface nonlinearity should decrease accordingly.

We consider here oxidation of a Si(111) surface as an example.[30] The experiment was carried out on a Si(111) wafer in an ultrahigh vacuum chamber. It contained - $10^{15}/cm^3$ phosphorous impurities. The sample surface was cleaned by heating at 1000°C for a few minutes. The appearance of a 7 × 7 LEED pattern was taken as a sign of nominal cleanliness. SHG from the Si surface was then measured with a 0.53 μm laser excitation. Soon after the surface was exposed to O_2, the SH signal decreased. Figure 9 shows SHG as a function of O_2 exposure in Langmuir units (1 L = 10^{-6} torr-sec). It is seen that at room temperature after - 90L, the signal drops to a saturation level of - 55% of the initial value. This saturation is an indication of the completion of a monolayer of O-atom coverage. Indeed, previous studies have established that at room temperature, O_2 chemisorbs to Si(111) and forms a monolayer at - 100L.[34] Thus, the result clearly depicts the submonolayer sensitivity of SHG for detecting oxygen adsorption.

At high temperatures, oxygen adsorption can persist beyond one monolayer to form multilayers of amorphous silicon oxides. However, since quenching of the dangling bonds is already complete, and the additional oxide layer has much lower nonlinearity, adsorption beyond one monolayer is not expected to change the SH signal significantly. This is seen in Fig. 9. At 800°C, a ~ 30L of oxygen exposure, corresponding to - 1 monolayer of oxygen coverage on Si(111) as calibrated by Auger spectroscopy

decreased the SH signal by ~ 55%. With 120L of exposure, the surface oxygen increased to 2 monolayer equivalents, but the signal changed only from ~ 55% to ~ 45%. Further increase of surface oxygen to 4 monolayer equivalents left the signal essentially unchanged. This clearly suggests that SHG is dominated by the first monolayer of chemisorbed oxygen.

We can also use SHG to monitor thermal desorption of oxygen from a Si surface. When a Si surface with 2 monolayer equivalents of chemisorbed oxygen was kept at 800°C in UHV, the SH signal first increased rapidly to ~ 50% of the clean value, corresponding to the desorption of the first oxygen monolayer, and thereafter, increased 5 times more slowly to the full clean value, corresponding to the desorption of the last oxygen monolayer. This result is expected from the higher binding energy for the chemisorbed oxygen that quenches a dangling bond.

The SH signal from the nominally clean Si(111) surface was found to decrease as the temperature was raised. At 800°C it dropped to ~ 50% of the room-temperature value. This change cannot be explained by the temperature dependence of the optical properties of Si. The Auger spectroscopy indicated that it was correlated to the segregation of the phorsphous impurities to the surface at room temperature and their diffusion back into the bulk at high temperatures. This suggests that SHG would increase with the surface coverage of P. However, because the sample contained only $10^{15}/cm^3$ of P impurities, the surface coverage of P could not be more than 2% of a monolayer. If the SHG could indeed respond to such a small number of surface P atoms, it would be most interesting to see whether this is also true for other impurities in Si and Ge.

VII. STUDY OF ADSORBATES ON METAL SURFACES

The high electron density gradient at a metal surface often leads to a large surface nonlinearity. As a result, SHG from a metal surface is generally much stronger than that from an insulator surface. Atomic or molecular adsorption may modify the surface electron distribution and change the surface nonlinearity. Alternatively, the adsorbates themselves may contribute significantly to the surface nonlinearity. In either case, the change in the SH signal can be used to monitor the presence of adsorbates and therefore, as a means to study the adsorbates.

We have already seen in Sec. IV that the adsorption of Cℓ and pyridine on an Ag electrode in an electrolytic solution can be detected by SHG. In both cases, the SH signal increases with the surface coverage of adsorbates. It is not yet understood why this is so. Clearly, results of SHG from the same adsorbates on a well-characterized Ag surface, namely, a crystalline Ag surface in UHV, will be very helpful. Unfortunately, this has not yet been done. Here, we shall discuss instead the case of atomic and molecular adsorption on a transition metal surface, Rh(111), studied by SHG.[16]

Transition metals are important in surface science because of their functions in catalytical reactions. We consider here adsorption of O_2, CO, and alkali metals on Rh(111). They are related to the catalytical reaction of hydrocarbon formation and oxidation, and have been studied to some extent by other techniques. They can therefore be used to gauge the potential of SHG as a UHV surface probe.

The experiment was conducted on a Rh(111) sample situated in a UHV chamber that was equipped with LEED, Auger, and mass spectrometer probes.

The base pressure of the chamber was 2×10^{-10} torr. The sample surface was cleaned with cycles of Ar^+ sputtering, heating at 200°C in 2×10^{-7} torr of O_2, annealing at 900°C in vacuum, and then flash-heating to 1000°C. The cleanliness of the surface was checked by Auger spectroscopy. Before an experiment, the sample was flash-heated to 1000°C again to remove CO adsorbed from the background and C and O deposited by the dissociation of CO during the Auger probing.

A. Adsorption of O_2 and CO on Rh(111)

In Fig. 10, we show how the SH signal from the Rh(111) surface at 315°K changes as a function of exposure to O_2. The signal drops monotonously from the bare metal value to the final 12% level at ~ 1.8L of O_2. As a calibration of the oxygen surface coverage, it is known that a saturated oxygen overlayer leads to a 2×2 LEED pattern,[35] which was observed at ~ 20L. Thus, the submonolayer sensitivity of SHG to the oxygen adsorption to Rh(111) is apparent. Since oxygen adsorbs to Rh in the atomic form,[36] this result shows that SHG can be used to monitor adsorption of atomic species on metals.

The experimental data in Fig. 10 can be fit by a theoretical calculation based on a model assuming noninteracting adsorption sites. Following this assumption, the surface nonlinear susceptibility of Rh with adsorbates can be written as

$$\chi_S^{(2)} = A + B\theta/\theta_S \qquad (22)$$

where A is the bare metal contribution, B is a constant, θ is the fractional surface coverage of oxygen with respect to Rh surface atoms, and

θ_S is the saturation value of θ. The adsorption rate should be governed by the Langmuir kinetics.[36] If the desorption rate is negligible, as in the present case, we have

$$\frac{d\theta}{dt} = \kappa p(1 - \theta/\theta_S) \tag{23}$$

where κ is a constant accounting for the sticking coefficient, and p is the oxygen pressure. Equation (23) yields

$$\theta = \theta_S[1 - \exp(-\kappa pt/\theta_S)]. \tag{24}$$

The SH signal is proportional to $|\chi_S^{(2)}|^2$, and therefore has the form

$$S \propto \left|1 + \frac{B}{A} - \frac{B}{A} e^{-\kappa pt/\theta_S}\right|^2. \tag{25}$$

Taking B/A and κ/θ_S as adjustable parameters, we can use Eq. (25) to fit the experimental data very well, as seen in Fig. 10. We find $B/A = 1.03 \exp(i160°)$ and $\kappa/\theta_S = 0.93L$. That the Langmuir kinetics indeed appears to describe the oxygen adsorption process confirms the earlier result of Yates et al. in their experiment using Auger spectroscopy as a probe.[36] Our value 0.93L for κ/θ_S is in fair agreement with their value 0.76L, considering the limited accuracy of the ion gauge used in the measurement of p. The constant κ is related to the sticking coefficient α by

$$\kappa = (\alpha/n_S)(RT/2\pi M_g)^{1/2} n_g \tag{26}$$

where n_S is the surface density of adsorption sites, R is the gas constant, T is the temperature, M_g is the molecular weight of the gas, and n_g is the density of the gas. If the adsorbed O atoms form a 2 × 2 saturated overlayer,[35] then $\theta_S = 0.25$ and the measured value of κ/θ_S yields $\alpha \sim 0.5$. It is also possible that the adsorbed O atoms actually form 3 domains of 2 × 1 overlayers with $\theta_S = 0.5$;[36] accordingly, the sticking coefficient will be close to 1.

The SH signal also decreased rapidly upon adsorption of CO on Rh(111), as shown in Fig. 11a. In this case, the $(\sqrt{3} \times \sqrt{3})R30°$ LEED pattern corresponding to $\theta = 1/3$ appeared at 1.2L of CO and the split (2 × 2 pattern corresponding to $\theta = \theta_S = 3/4$ appeared at ~ 11L of O_2.[35] We can then use the LEED patterns as the calibration points to convert the curve in Fig. 11b to SHG versus surface coverage of CO. The result exhibits a rather sudden change in the slope at $\theta = 1/3$. This suggests that the CO adsorption sites on Rh may be different for $\theta < 1/3$ and $\theta > 1/3$. Actually, previous studies[37] by electron energy loss spectroscopy have already established that CO adsorbs to Rh(111) on the top sites if $\theta < 1/3$, and on both top and bridge sites if $\theta > 1/3$. Assuming noninteracting adsorption sites, we can write the surface nonlinear susceptibility as

$$\chi_S^{(2)} = A + B\theta/\theta_S \qquad \text{for } \theta \leq 1/3$$

$$= A + B/3\theta_S + C(\theta - 1/3)/\theta_S \qquad \text{for } 1/3 \leq \theta \leq 3/4 \qquad (27)$$

where A is the bare metal contribution, and B and C are constants charac-

terizing the contributions from CO adsorbed at top and bridge sites, respectively. With B/A and C/A taken as adjustable parameters, the expression for the SH signal, $S \propto |\chi_S^{(2)}|^2$ following Eq. (27), can describe the experimental data very well as seen in Fig. 11b. The result indicates that SHG as a surface probe can even be site-specific.

One may ask why the SH signal from Rh(111) should decrease upon adsorption of O_2 or CO. This can be understood from the following reasoning. The surface nonlinearity of a metal is often dominated by the delocalized electrons at the surface. It is relatively high because of the high surface electron density and its strong gradient along the surface normal.[38] Oxygen and CO are electron acceptors. Their adsorption on a metal surface would localize part of the delocalized electrons. As a result, the surface nonlinearity would decrease as long as the adsorbed species is less nonlinear than the metal surface. If this is true, we should anticipate an increase in the surface nonlinearity with the adsorption of electron donors on a metal. Alkali atoms are known to be effective electron donors. It is therefore interesting to see how SHG varies with the adsorption of alkali atoms on Rh(111).

B. Adsorption of Na, K, and Cs on Rh(111)

Alakli atoms are also known as promoters for catalytical reactions.[2] Their ability to improve the performance of catalysis on metal surfaces is directly related to electron donation. For example, in the case of CO on Rh, the back donation of electrons from the metal to the $2\pi^*$ antibonding orbital of CO weakens the CO bond. This is the basis of catalytical reactions involving CO on Rh. The adsorption of alkali atoms on CO/Rh further enhances the back donation of electrons and promotes the

catalytical reactions.

We should expect the delocalized surface electron density on Rh(111) to increase upon adsorption of alkali atoms, and consequently, the surface SHG to increase. Indeed, as shown in Fig. 12, the observed SH signal from Rh(111) rises sharply when only a small fraction of a monolayer of Na, K, or Cs appears on Rh. One monolayer here refers to the hexagonal close-packed structure monitored by LEED with $\theta_S = 0.5$ for Na and $\theta_S = 0.35$ for K and Cs. For $0.3 \leq \theta/\theta_S \leq 2$, the curves in Fig. 12 show a rather complex behavior. In this region, the adsorbed alkali atoms are presumably neutral; they interact and gradually form a metallic film.[39] The plasmon resonance frequency increases from one associated with electron-enhanced transition metal surface to that of the pure alkali metal surface.[40] The variation of the SH signals in Fig. 13 is believed to be due to the dispersive effect in the SHG as ω_p sweeps over the fundamental and second-harmonic frequencies. For $\theta/\theta_S \gtrsim 2$, the SH signal from the alkali-metal-covered Rh(111) is essentially constant. This indicates that SHG is now dominated by the two surface monolayers of alkali metal. It is therefore another demonstration of the surface specificity of SHG. Since Cs is better than K, and K better than Na, as a free-electron metal, the SHG from the alkali metal surfaces is expected to have the signal strength follow the same order. This is confirmed in Fig. 12.

One may find it surprising that the SH output in Fig. 12 increases by 100 times when only 1/3 monolayer of alkali atoms is adsorbed to the Rh(111) surface. The adsorbed alkali atoms could not have increased the surface electron density by 10 times. Therefore, the increase of the

surface nonlinearity must not result only from the change in the surface electron density. We believe that the adsorption of individual alkali atoms on Rh allows electrons to move quite freely between the atoms and the surface, and thus create a giant nonlinearity on the surface.

C. Co-adsorption of CO and Na on Rh(111)

As we already mentioned, the adsorption of CO on Rh(111) should be affected by the preadsorption of Na on the surface. This can also be monitored by surface SHG. Figure 13a shows how the SH signal varies with the CO exposure in the presence of 0.6 monolayer of Na on Rh(111). In comparison with the curve in Fig. 11a for CO exposure of clean Rh(111), we notice that the curve in Fig. 13a starts with a step and then drops more sharply. It suggests that there are three different adsorption sites for CO: the top site, the bridge site, and a site next to Na.[41] These three sites should of course have different binding energies which can be estimated from the thermal desorption temperatures of the CO species. In the desorption experiment, the Rh(111) surface was first covered by 0.6 monolayer of Na and then saturated by CO. The sample was then heated up to effect the desorption of various species. Figure 13b describes how the SH signal varies with the surface temperature. The curve shows that four different species seem to have been desorbed in the process. This is seen more clearly by comparing the signal levels of Figs. 13a and 13b at various points. The four species are CO at the top and bridge sites (desorbed between 200 and 400°C and between 400 and 500°C), CO at sites next to Na (desorbed between 500 and 600°C), and Na (desorbed between 600 and 800°C). Above 800°C, the Rh(111) surface appears to be clean. We should also remark that SHG here

responds to what is still left on the surface in a desorption process. It could therefore be a useful complement to the well known thermal desorption spectroscopy.

The preadsorption of Na on Rh can block off the adsorption sites for CO.[41] This is most easily seen when the Rh(111) surface is first covored by a monolayer of Na and the SHG is then used to monitor the CO adsorption as a function of CO exposure. Figure 14 shows that even after 1000L exposure, the SH signal decreases by only 20%. In contrast, the SH signal in Fig. 11a drops to less than 40% after only 1L exposure of clean Rh(111) to CO. The result is a clear demonstration that CO adsorption on Rh(111) is indeed effectively blocked by the preadsorption of Na. In another measurement, we found that a preadsorption of 1.3 monolayer of Na on Rh(111) could completely block off the adsorption of CO as the SH signal became absolutely independent of the CO exposure.

VIII. CONCLUDING REMARKS

There are clearly many other surface science problems that can be studied by SHG. For example, one can use SHG to measure the orientation of surfectant molecules at air/liquid, liquid/liquid/ and air/solid interfaces,[42] to probe two-dimensional orientational phase transitions, to study epitaxial growth and the formation of solid/solid interfaces, to monitor surface reactions, and so on. Evidence is mounting the SHG is indeed a powerful tool for surface studies. This is especially true considering the fact that few existing surface probes can be used for in-situ measurements on surfaces outside a vacuum chamber.

Among the numerous advantages that surface SHG can offer, the most

attractive one is the time resolution, which, in principle, is limited only by the laser pulsewidth. With femptosecond laser pulses, we could now study changes on a surface with a femptosecond time resolution. This is most exciting because the method would allow us to investigate many interesting and important problems of surface dynamics. So far, limited by techniques, surface science research has not made much progress in this important subarea. Hopefully, surface SHG could modify the trend.

The major disadvantage of SHG as a surface tool is the lack of spectral selectivity. As we discussed in Sec. VA, the technique can be used to probe the electronic transitions of molecular adsorbates. However, the spectral widths of these transitions are often too broad to be useful in distinguishing different adsorbed species of similar structures. Extension of the technique to sum-frequency generation with a tunable infrared laser excitation is clearly the solution since the vibrational modes of the adsorbates can then be probed. Unfortunately, the tunability of medium-power pulsed lasers in the infrared is still quite limited. It is particularly difficult to achieve in the far-infrared range (> 10 μm) where many molecular vibrational modes happen to be. The situation can hopefully be changed when the infrared free electron lasers become operative.

Another difficulty of SHG as a surface tool is the lack of theoretical understanding of the surface nonlinearity. It is not yet clear to us how the microscopic properties of various surfaces are related to their surface nonlinearities. Such an understanding would be most helpful in making SHG more effective as a surface probe because we could then

use SHG to study, for example, how the surface electronic properties are changed even during the adsorption of atoms or molecules. This is undoubtedly a very challenging problem. Its solution would proably require a close collaboration between theory and experiment.

ACKNOWLEDGEMNET

The author has benefited from discussion and collaboration with G. T. Boyd, C. K. Chen, T. F. Heinz, Th. Rasing, D. Ricard, H. W. K. Tom, P. Ye, and X. D. Zhu. Without their contributions, the recent development of optical second harmonic generation for surface studies would be impossible. This work was supported by the Director, Office of Energy Research, Office of Basic Energy Sciences, Materials Sciences Division of the U.S. Department of Energy under Contract Number DE-AC03=76SF00098.

REFERENCES

1. See, for example, Surface Studies with Lasers, eds. F. R. Aussenegg, A. Leitner, and M. E. Lippitsch (Springer-Verlag, Berlin, 1983).

2. See, for example, G. Somorjai, Chemistry in Two Dimensions: Surfaces (Cornell University Press, Ithaca, NY, 1981).

3. See, for example, J. Hager, Y. R. Shen, and H. Walther, in Proceedings of International Conference on Laser Processing and Diagnostics, Linz, Austria, July, 1984 (Springer-Verlag, Berlin, 1984), and references therein.

4. T. J. Chuang and H. Seki, Phys. Rev. Lett. 49, 382 (1982).

5. F. Trager, H. Coufal, and T. J. Chuang, Phys. Rev. Lett. 49, 1720 (1982).

6. A. C. Boccara, D. Fournier, and J. Badoz, Appl. Phys. Lett. 36, 130 (1980); M. A. Olmstead and N. M. Amer, Phys. Rev. Lett. 52, 1148 (1984).

7. B. F. Levine, C. V. Shank, and J. P. Heritage, IEEE J Quant. Electron. QE-15, 1418 (1979).

8. J. P. Heritage and D. L. Allara, Chem. Phys. Lett. 74, 507 (1980).

9. C. K. Chen, A. R. B. de Castro, Y. R. Shen, and F. DeMartini, Phys. Rev. Lett. 43, 946 (1979).

10. See, for example, Y. R. Shen, The Principles of Nonlinear Optics (J. Wiley, New York, 1984), Ch. 25.

11. J. M. Chen, J. R. Bower, C. S. Wang, and C. H. Lee, Optics Comm. 9, 132 (1973).

12. C. K. Chen, T. F. Heinz, D. Ricard, and Y. R. Shen, Phys. Rev. Lett. 46, 1010 (1981).

13. T. F. Heinz, C. K. Chen, D. Ricard, and Y. R. Shen, Phys. Rev. Lett. 48,

478 (1982).

14. T. F. Heinz, H. W. K. Tom, and Y. R. Shen, Phys. Rev. A 28, 1883 (1983).

15. H. W. K. Tom, T. F. Heinz, and Y. R. Shen, Phys. Rev. Lett. 51, 1983 (1983).

16. H. W. K. Tom, C. M. Mate, X. D. Zhu, J. E. Crowell, T. F. Heinz, G. Somorjai, and Y. R. Shen, Phys. Rev. Lett. 52, 348 (1984).

17. N. Bloembergen and P. S. Pershan, Phys. Rev. 128, 606 (1962).

18. C. C. Wang, Phys. Rev. 178, 1475 (1969).

19. P. Ye and Y. R. Shen, Phys. Rev. B 28, 4288 (1983).

20. C. K. Chen, T. F. Heinz, D. Ricard, and Y. R. Shen, Phys. Rev. B 27, 1965 (1983).

21. See, for example, Surface Enhanced Raman Scattering, eds. R. K. Chang and T. E. Furtak (Plenum Press, New York, 1982).

22. C. K. Chen, A. R. B. de Castro, and Y. R. Shen, Phys. Rev. Lett. 46, 145 (1981); G. T. Boyd, Th. Rasing, J. R. R. Leite, and Y. R. Shen, Phys. Rev. B 30, 519 (1984).

23. C. K. Chen, T. F. Heinz, D. Ricard, and Y. R. Shen, Chem. Phys. Lett. 83, 455 (1981); G. L. Richmond, Chem. Phys. Lett. 106, 26 (1984).

24. R. M. Corn, M. Romagnoli, M. D. Levenson, and M. R. Philpott, Chem. Phys. Lett. 106, 30 (1984); R. Richmond, Chem. Phys. Lett. (to be published).

25. G. Marowsky (private communication).

26. See, for example, H. Ibach and D. L. Mills, Electron Loss Spectroscopy and Surface Vibrations (Academic Press, New York, 1982).

27. H. W. K. Tom, Ph.D. Thesis, Univ. of Calif., Berkeley, 1984 (unpublished).

28. S. J. Lalama and A. F. Garito, Phys. Rev. A 20, 1179 (1979).

29. P. DiLazzaro, P. Mataloni, and F. DeMartini, XIIIth Internatl. Quantum Electron. Conf., Anaheim, Calif., June, 1984, paper MHH4.

30. H. W. K. Tom, X. D. Zhu, Y. R. Shen, and G. A. Somorjai, Proc. XVII Internatl. Conf. on the Physics of Semiconductors, San Francisco, CA, 1984, paper TuP-PC7.

31. C. V. Shank, R. Yen, and C. Hirlimann, Phys. Rev. Lett. 51, 900 (1983).

32. S. A. Akhmanov, N. I. Koroteev, G. A. Paitian, I. L. Shumay, M. F. Galjantdinov, I. B. Khaibullin, and E. I. Shtyrkov, Optics Commun. 47, 202 (1983).

33. T. F. Heinz, M. M. T. Loy, and W. A. Thompson, Conf. on Lasers and Electro-optics, Anaheim, Calif., June, 1984, paper PD1-1.

34. J. Onsgaard, W. Heiland, and E. Taglauer, Surf. Sci. 99, 112 (1980).

35. D. G. Castner, B. A. Sexton, and G. A. Somorjai, Surf. Sci. 71, 519 (1978).

36. J. T. Yates, P. A. Thiel, and W. H. Weinberg, Surf. Sci. 82, 45 (1979).

37. M. A. Van Hove, R. J. Koestner, and G. A. Somorjai, Phys. Rev. Lett. 50, 903 (1982), and references therein.

38. See, for example, Y. R. Shen, The Principles of Nonlinear Optics (J. Wiley, New York, 1984), Ch. 1.

39. S. A. Lindgren and L. Wallden, Phys. Rev. B 22, 5969 (1980).

40. U. Jostell, Surf. Sci. 82, 333 (1979).

41. J. E. Crowell, E. L. Garfunkel, and G. A. Somorjai, Surf. Sci. 121, 303 (1982); M. P. Miskinova, Surf. Sci. 111, 584 (1981); G. Broden, G. Gafner, and H. P. Bonzel, Surf. Sci. 84, 295 (1979); J. E. Crowell, E. L. Garfunkel, and G. A. Somorjai (to be published).

42. Th. Rasing, M. W. Kim, and Y. R. Shen (to be published).

FIGURE CAPTIONS

Fig. 1 A three-layer system representing the interface between two bulk media.

Fig. 2 Experimental arrangement of second harmonic generation from a surface.

Fig. 3 Second harmonic generation from a smooth Ag surface (lower curve) and from a roughened Ag surface (upper curve) as a function of input laser power. The quadratic power dependence of the output on the input is characteristic of the second harmonic generation process.

Fig. 4 Current and diffuse second harmonic signal as functions of time during and after an electrolytic cycle. The voltages listed on the lower curve are the potential of the Ag electrode with respect to a saturated calomel electrode. 0.05 M pyridine was added to the 0.1 M KCℓ solution following the completion of the electrolytic cycle.

Fig. 5 Resonant second harmonic generation in rhodamine 110 and rhodamine 6G. (a) Indicates the resonant process in the two dyes with energy levels corresponding to the absorption line centers for the molecules dissolved in ethanol. (b) Shows the experimental SH spectra in the region of the $S_0 \rightarrow S_2$ transition for submonolayers of the dye molecules adsorbed on fused silica.

Fig. 6 Structure of p-nitrobenzoic acid (PNBA) as a free molecule (a) and in its chemisorbed form (b).

Fig. 7 Isotherm for adsorption of PNBA on fused silica out of an ethanol solution. The results were deduced from the SH intensity under

s-polarized excitation at 532 nm.

Fig. 8 Second harmonic radiation from a Si(111) surface versus angle of rotation about the surface normal for p-polarized input excitation and (a) $\hat{s}$-polarized output, and (b) $\hat{p}$-polarized output. The dashed curves are theoretical fits to the experimental results (solid curves).

Fig. 9 Second harmonic generation during oxidation of Si(111) surface at room Temperature (RT, ___) and at 800°C (—-).

Fig. 10 Second harmonic generation from Rh(111) during O_2 exposure. ___, experimental result, —-, theoretical fit.

Fig. 11 (a) Second harmonic generation from Rh(111) during CO exposure. LEED patterns were observed at the exposures noted. (b) Second harmonic generation from CO/Rh(111) as a function of CO fractional coverage. Circles are experimental points and the solid curve is a theoretical fit.

Fig. 12 Second harmonic generation from Rh(111) versus surface coverage of Na, K, and Cs. The laser excitation was at 1.06 μm.

Fig. 13 Second harmonic generation from Rh(111) predeposited with 0.6 monolayer of Na, (a) during CO exposure, and (b) during the thermal desorption process after the surface was exposed to ~ 15L of CO.

Fig. 14 Second harmonic generation from Rh(111) predeposited with 1 monolayer of Na as the surface was exposed to CO.

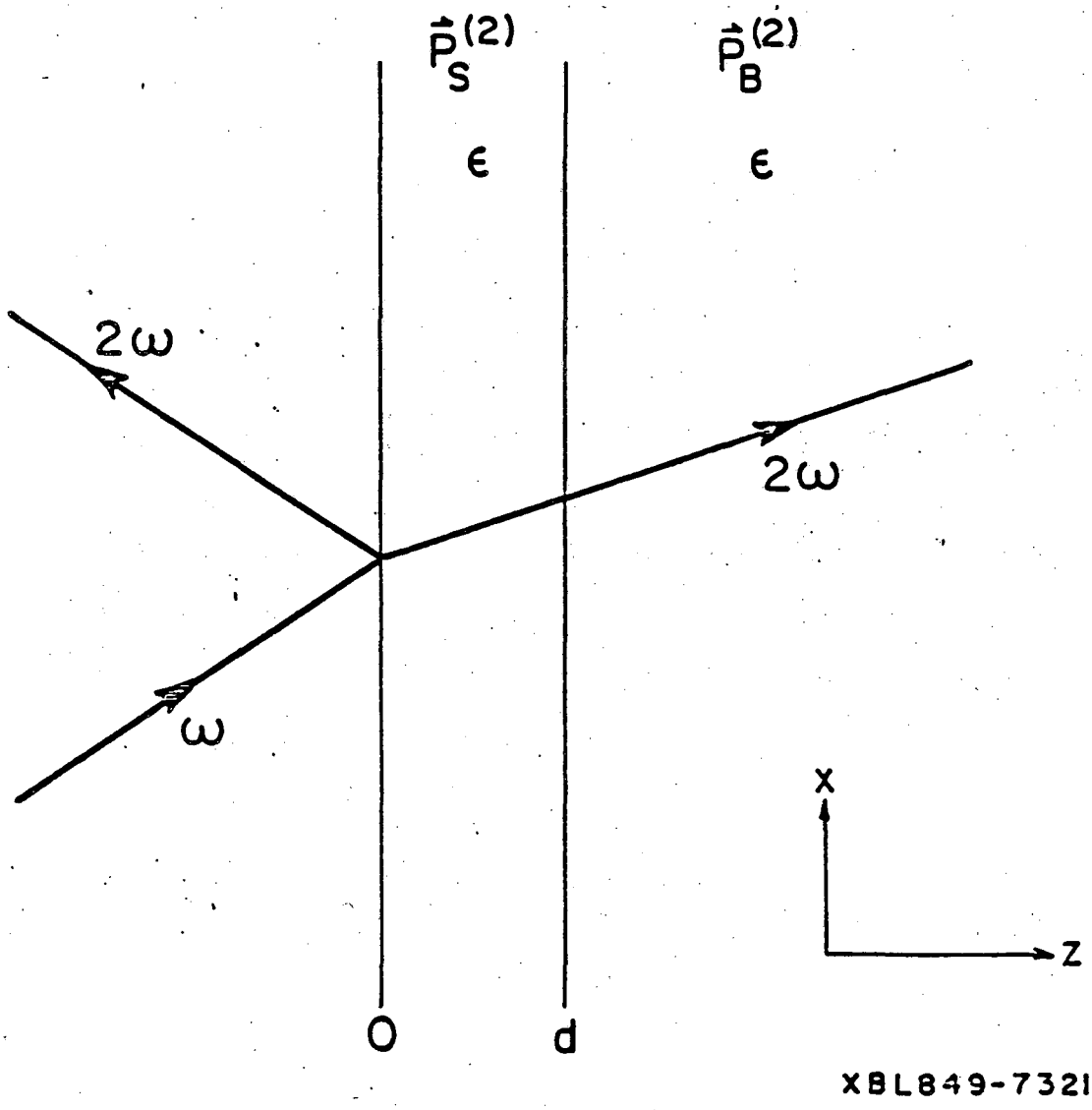

Fig. 1

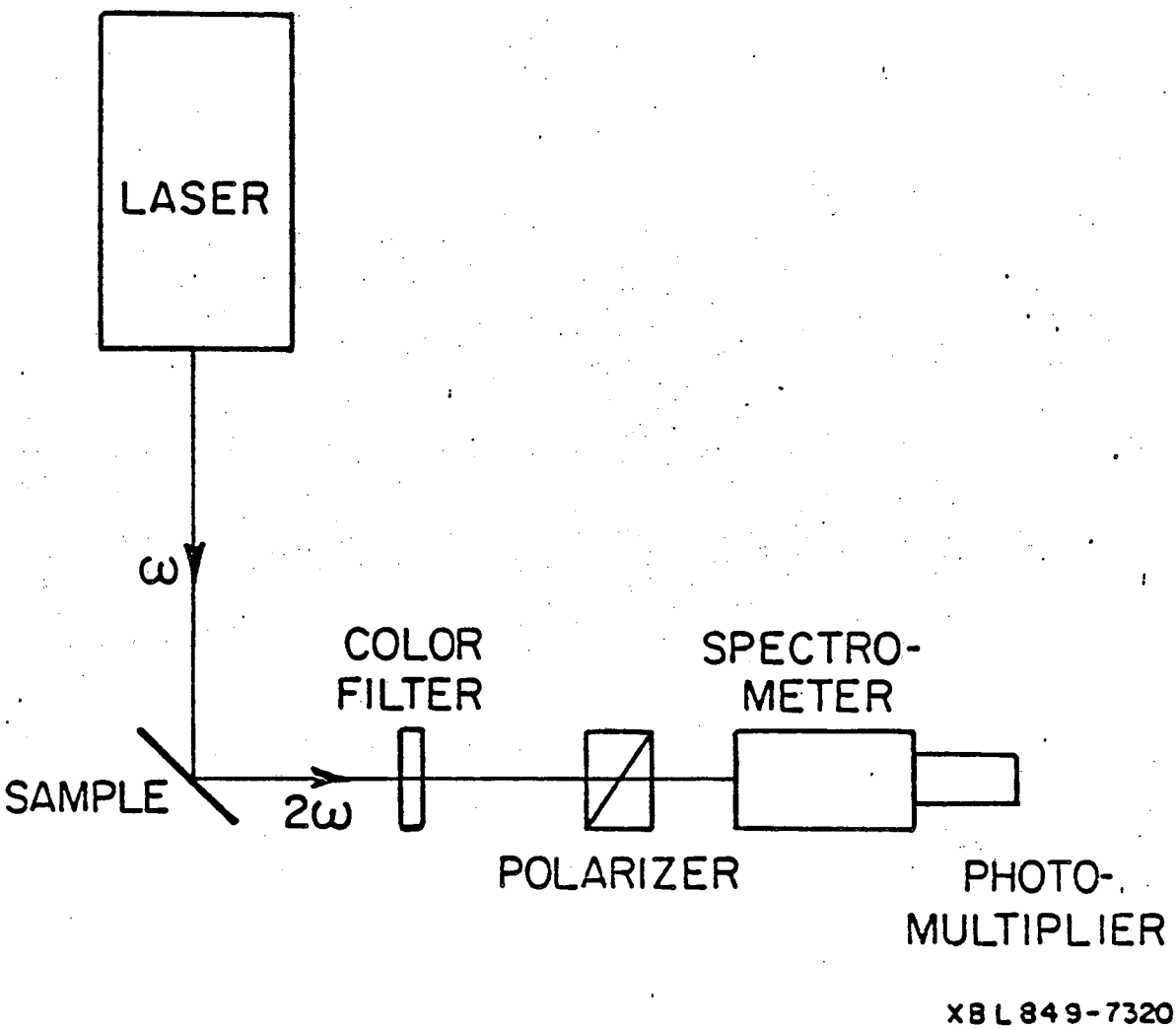
LASER
ω
COLOR
FILTER
SPECTRO-
METER
SAMPLE
2ω
POLARIZER
PHOTO-
MULTIPLIER
XBL849-7320

Fig. 2

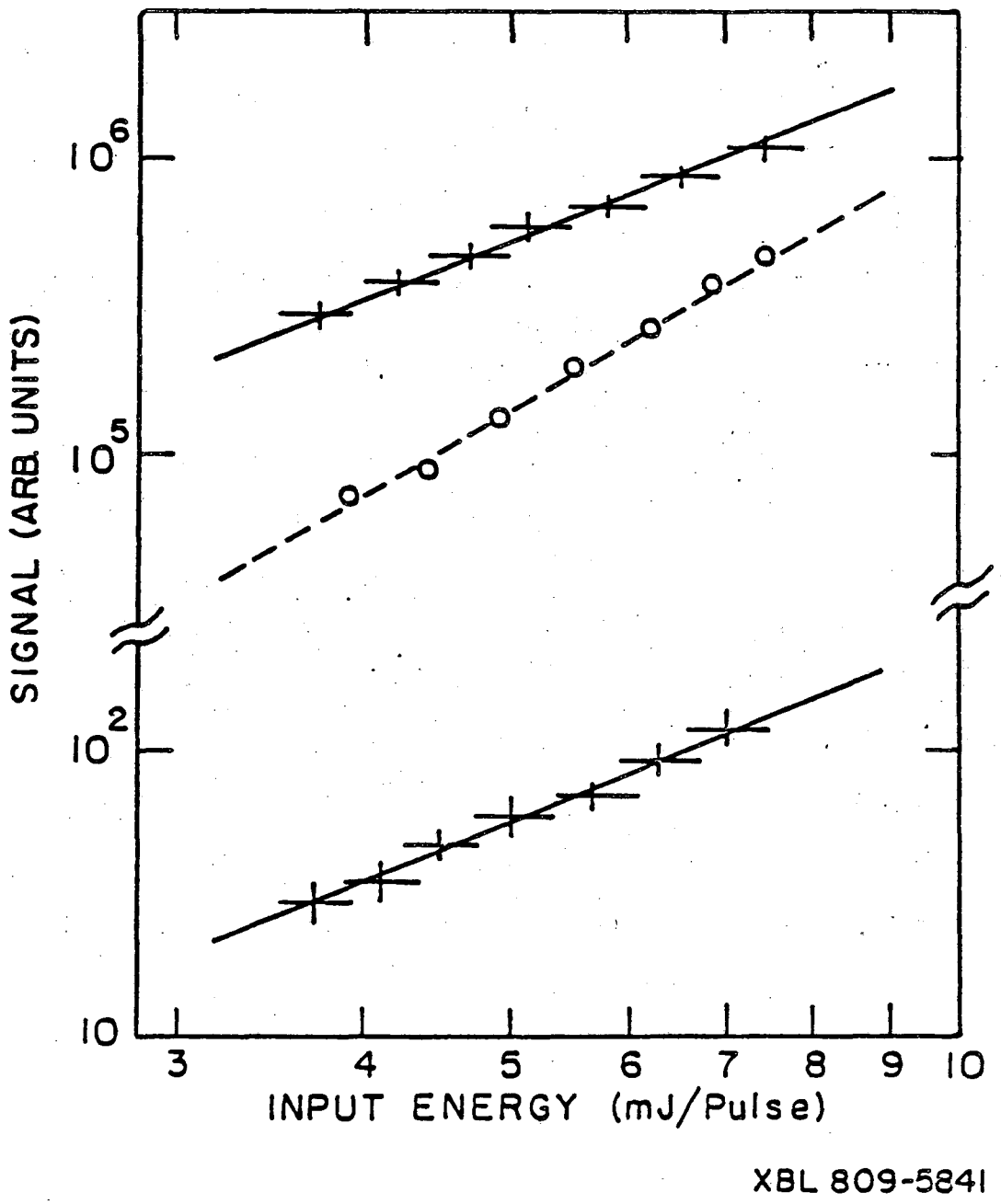
SIGNAL (ARB. UNITS)
10^6
10^5
10^2
10
3
4
5
6
7
8
9
10
INPUT ENERGY (mJ/Pulse)
XBL 809-5841

Fig. 3

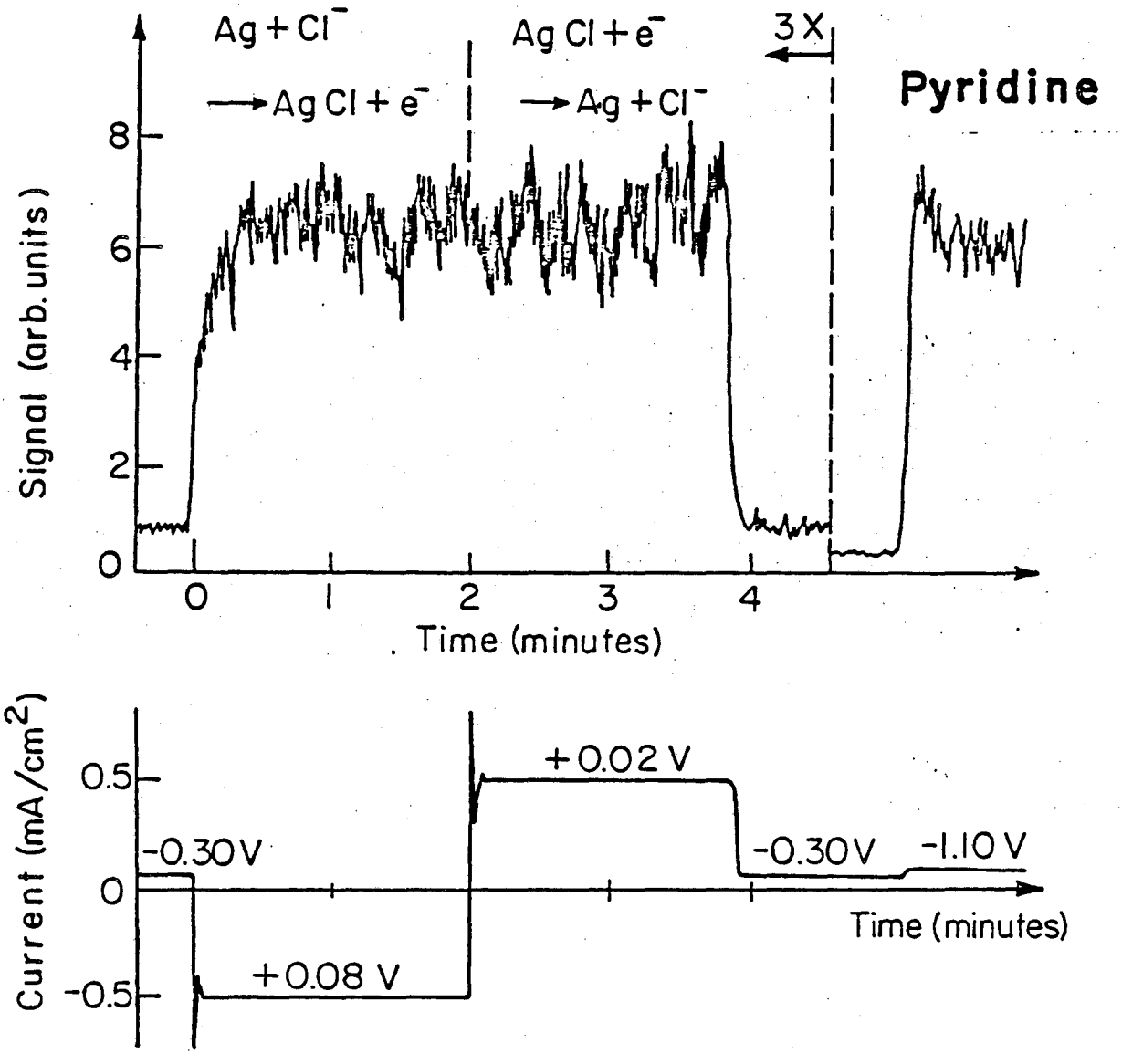

XBL 8012-13338

Fig. 4

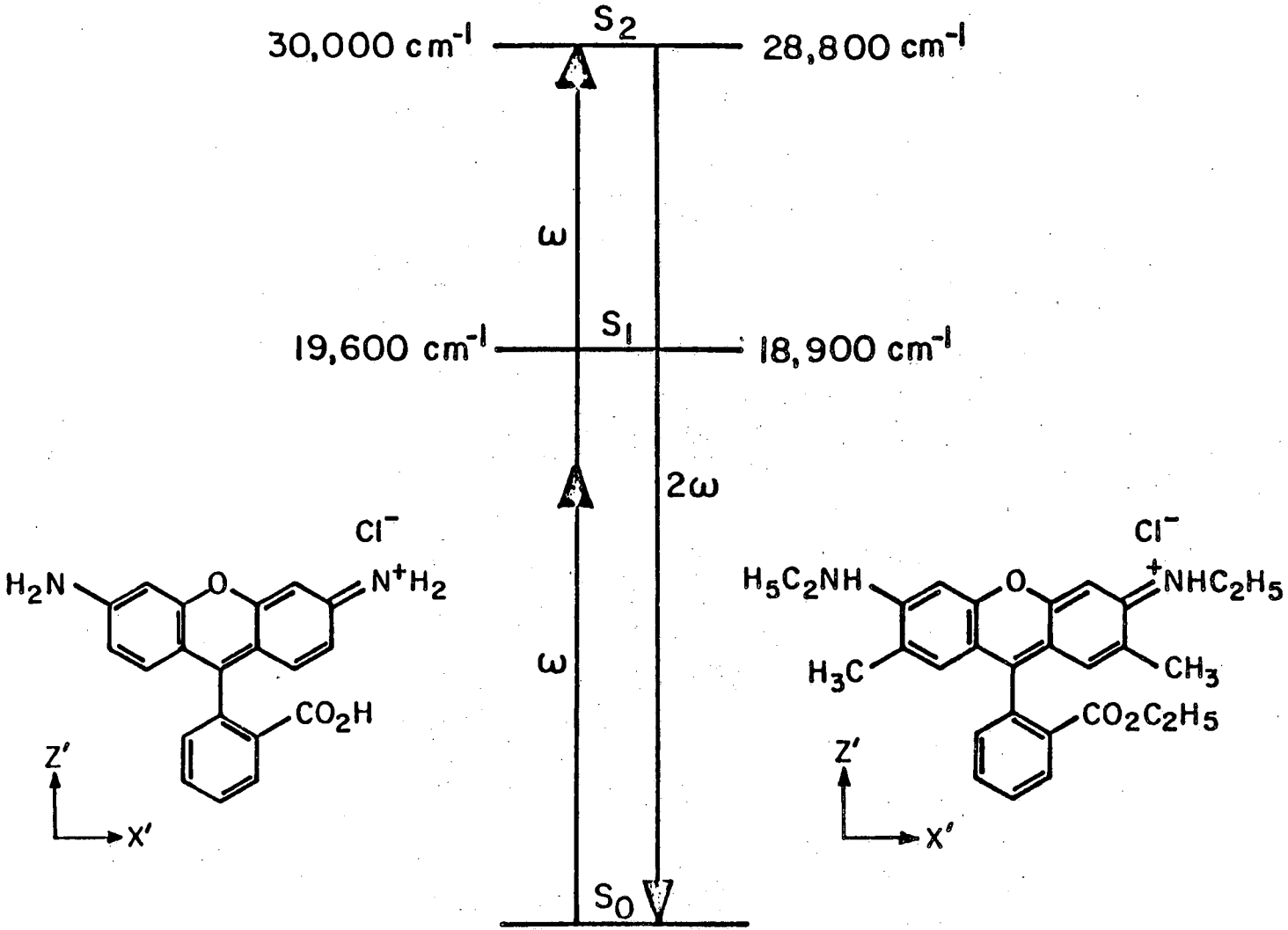

Rhodamine 110

Rhodamine 6G

XBL8111-12843

Fig. 5(a)

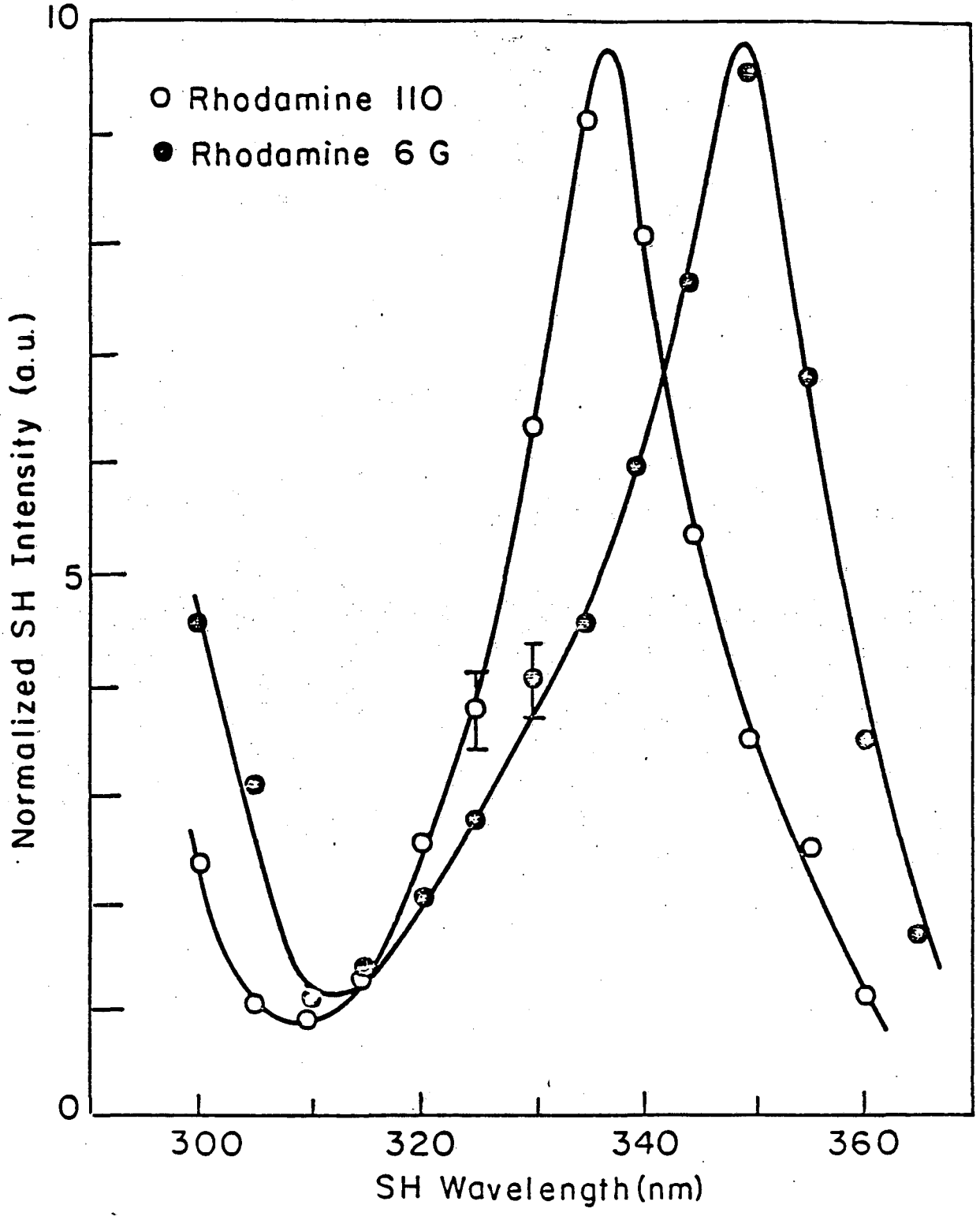
10
5
0
Normalized SH Intensity (a.u.)
O Rhodamine 110
● Rhodamine 6 G
300
320
340
360
SH Wavelength (nm)
XBL 8110-6773

Fig. 5(b)

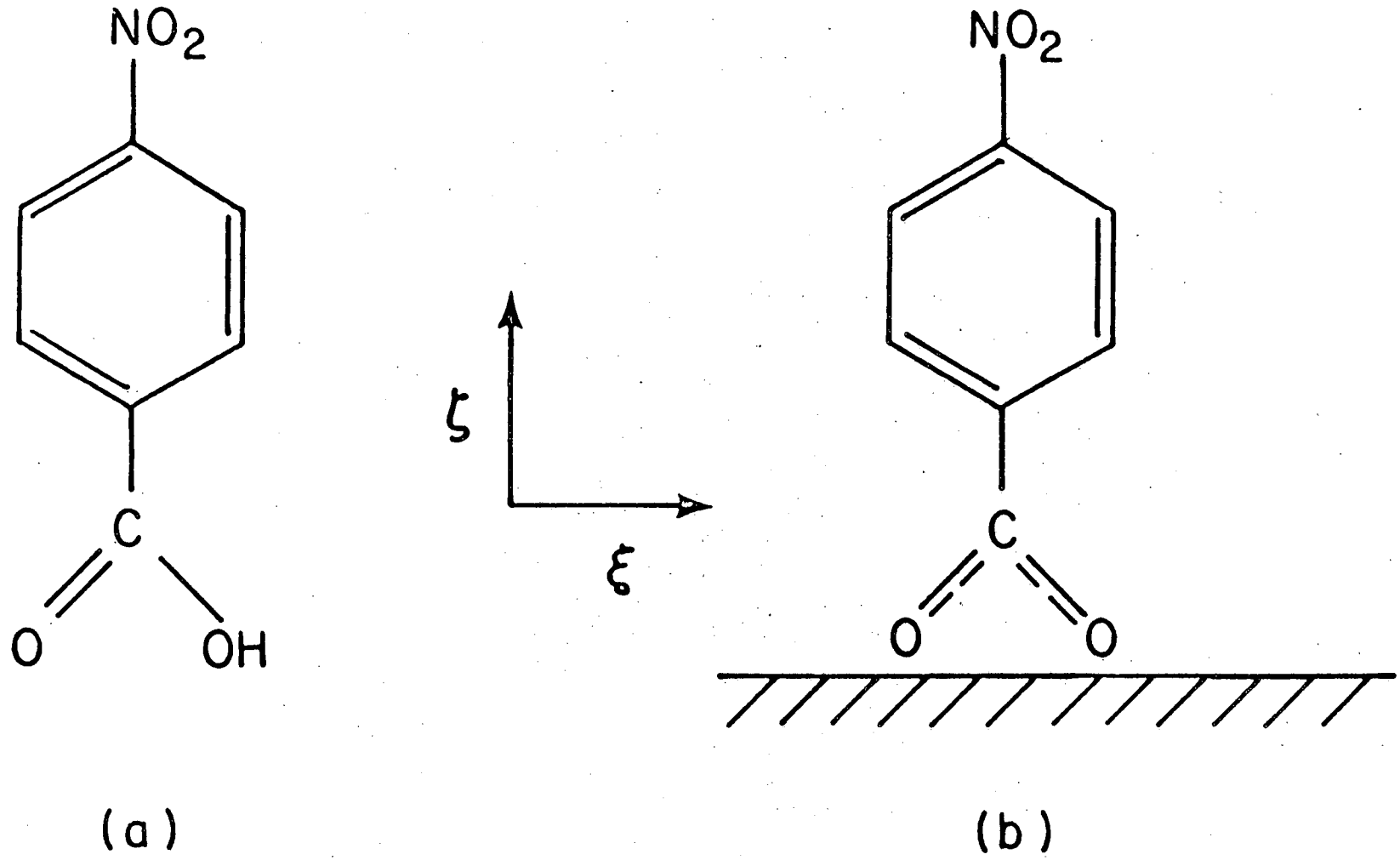

XBL 8212-7390

Fig. 6

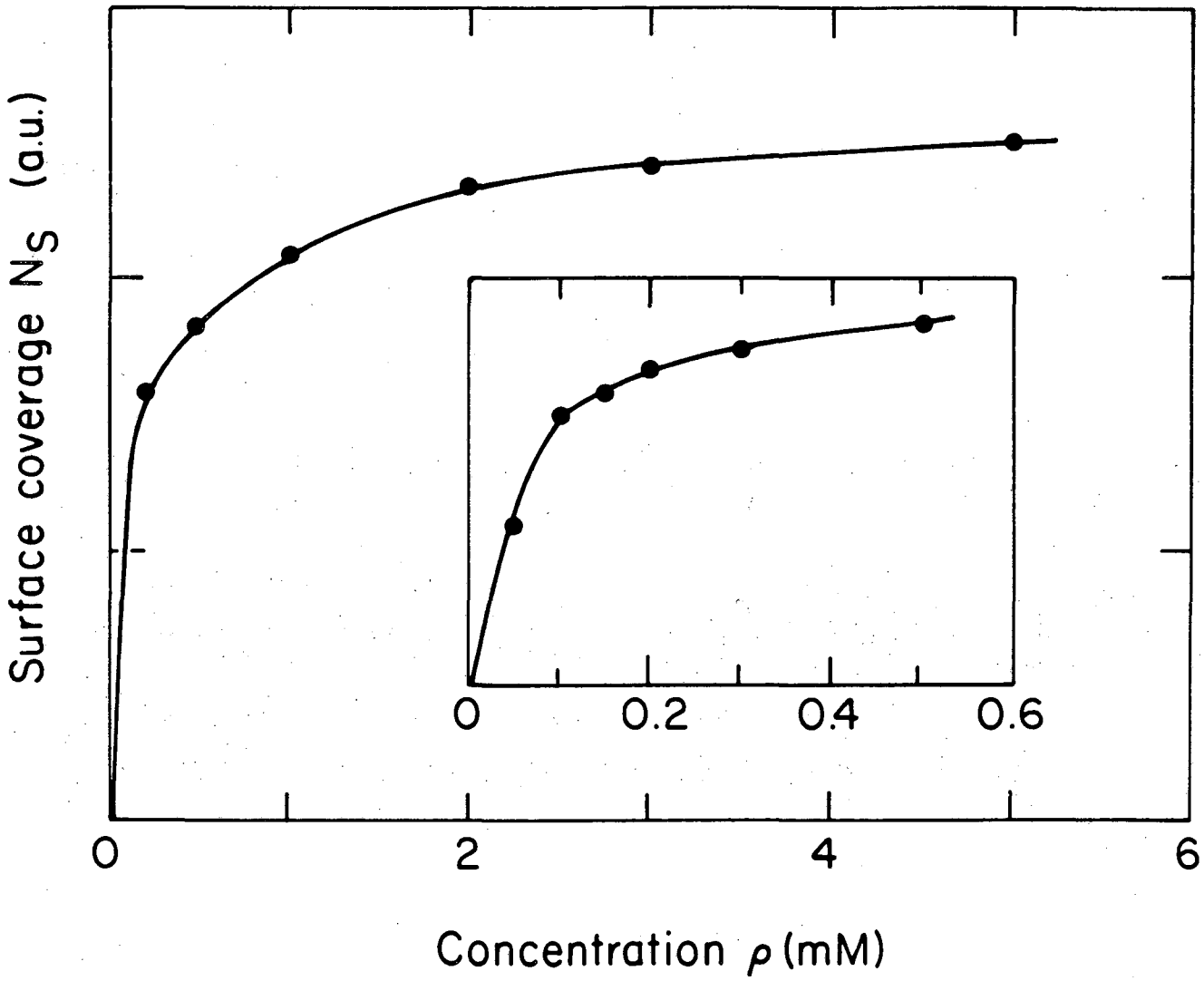

XBL8212-7391

Fig. 7

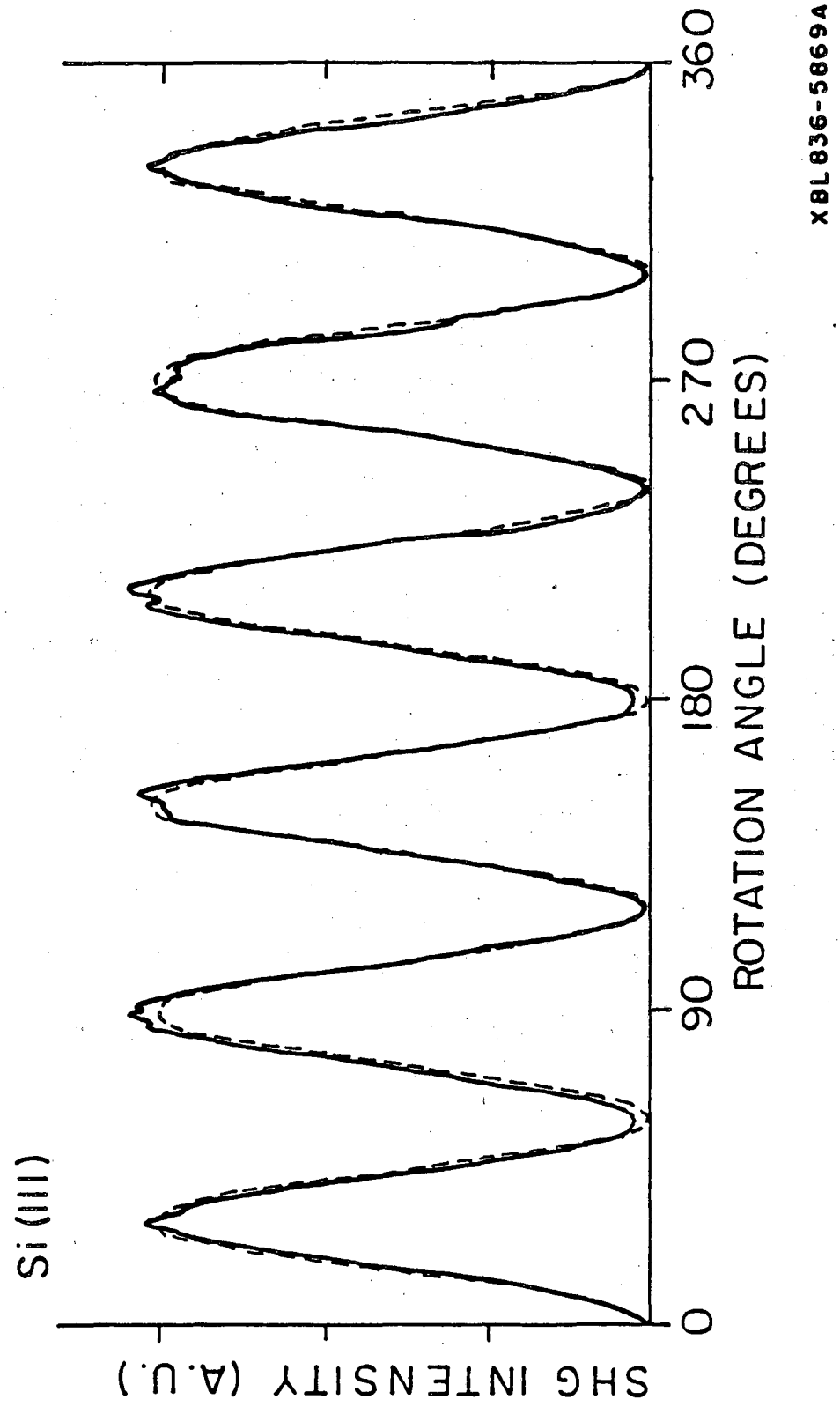
Si (111)
SHG INTENSITY (A.U.)
0
90
180
270
360
ROTATION ANGLE (DEGREES)
XBL836-5869A

Fig. 8(a)

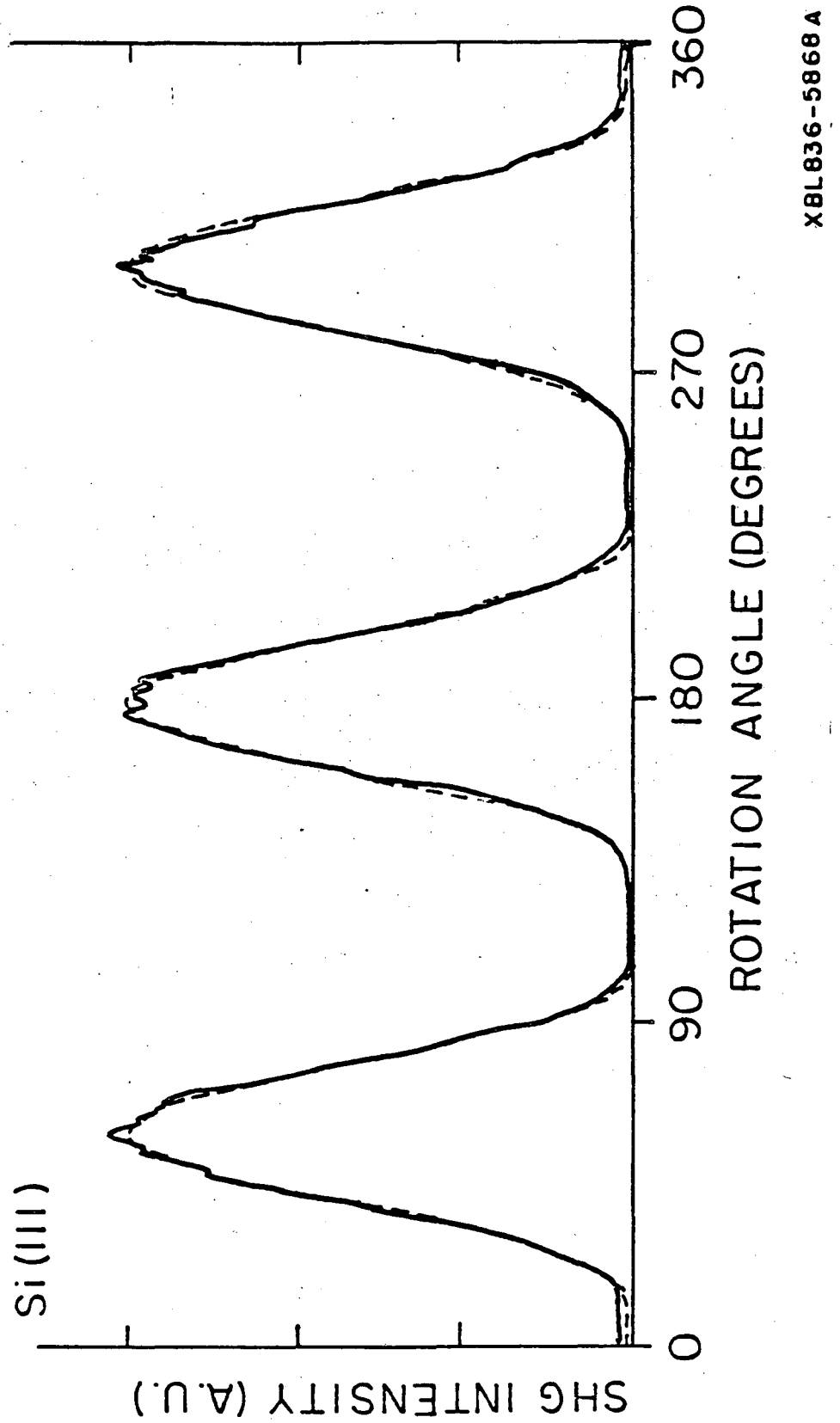
Si (111)
SHG INTENSITY (A.U.)
0
90
180
270
360
ROTATION ANGLE (DEGREES)
XBL836-5868A

Fig. 8(b)

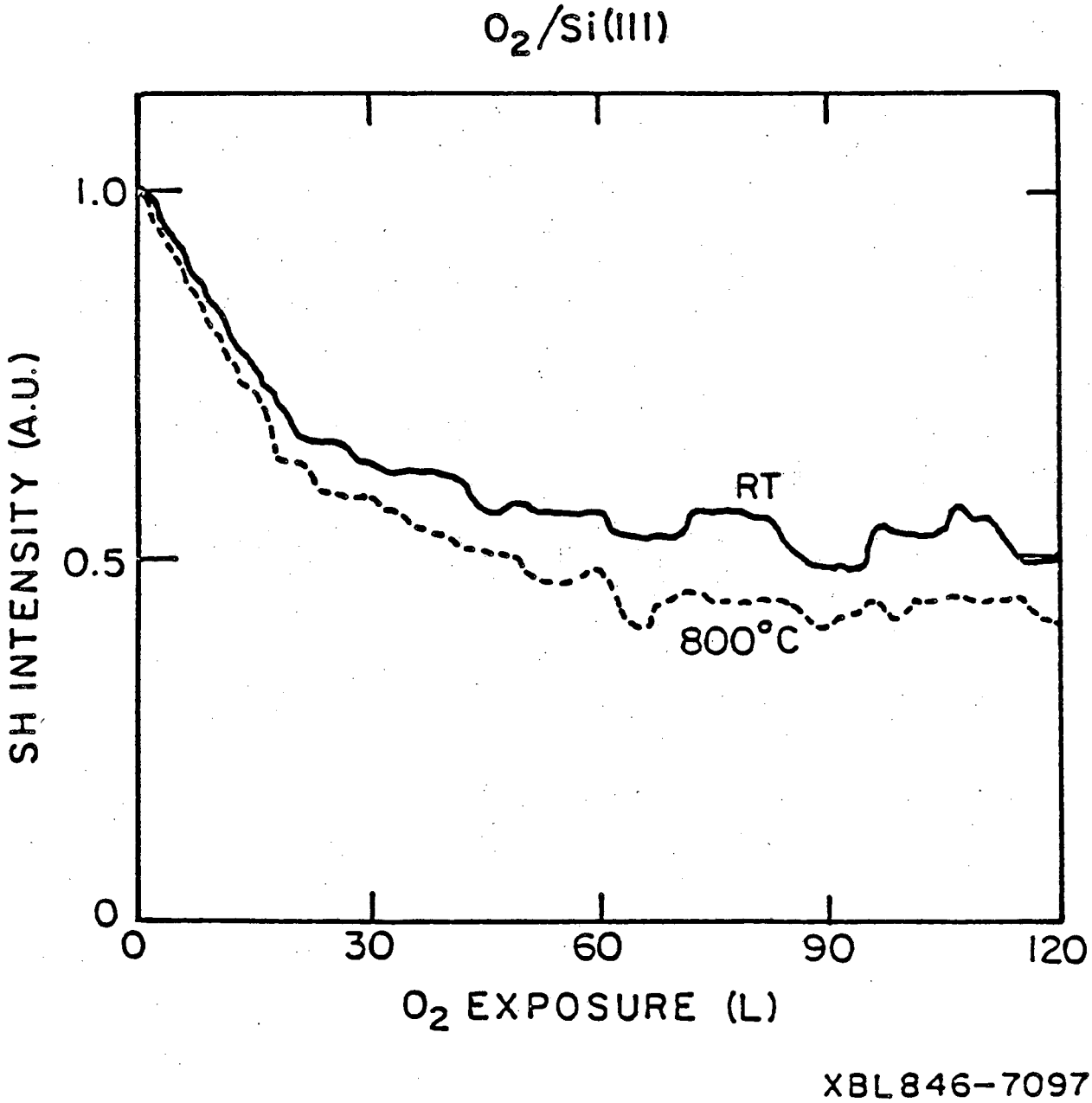
O_2/Si(111)
1.0
0.5
0
SH INTENSITY (A.U.)
RT
800°C
0
30
60
90
120
O_2 EXPOSURE (L)
XBL846-7097

Fig. 9

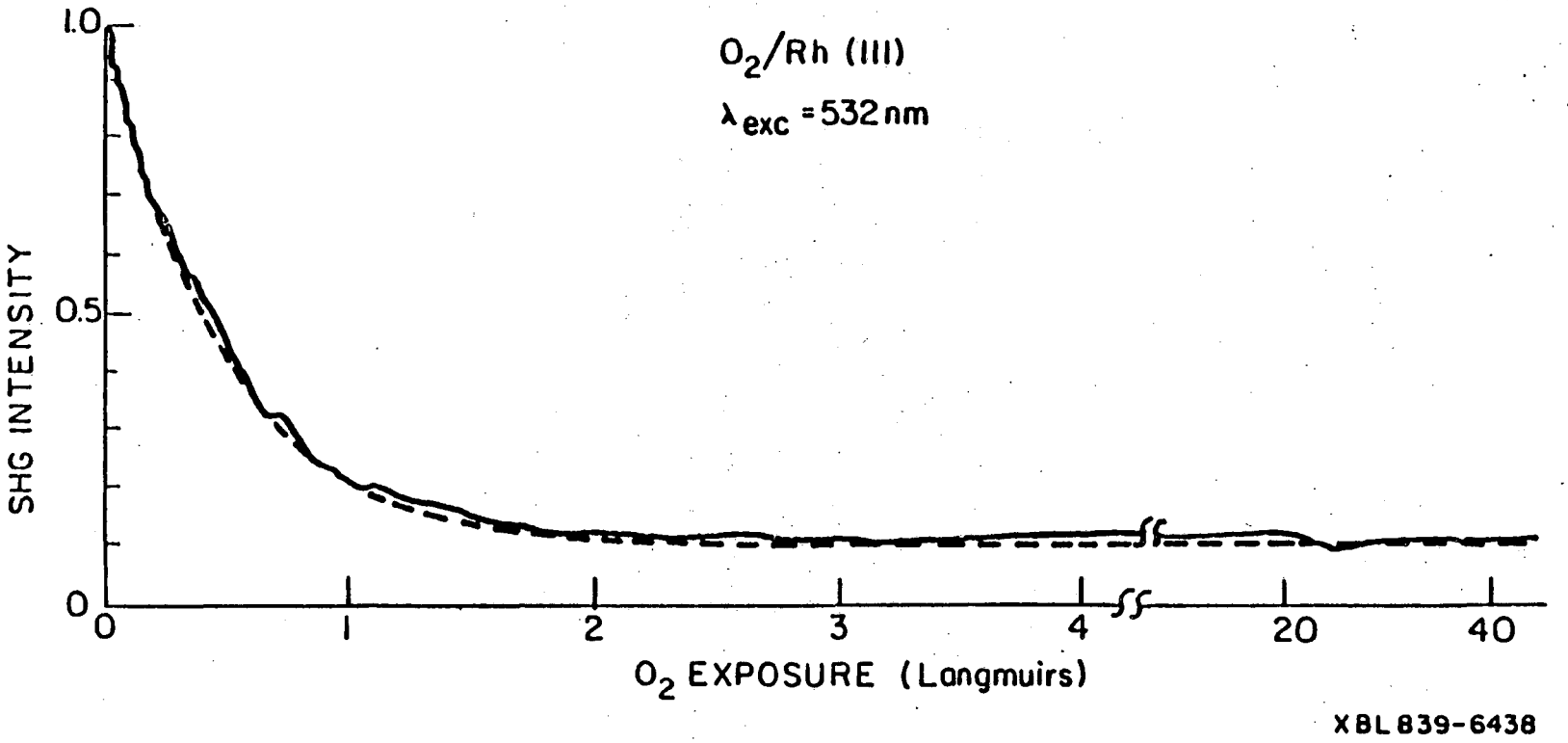
1.0
0.5
0
SHG INTENSITY
O_2/Rh (111)
λ_{exc} = 532 nm
0
1
2
3
4
20
40
O_2 EXPOSURE (Langmuirs)
XBL 839-6438

Fig. 10

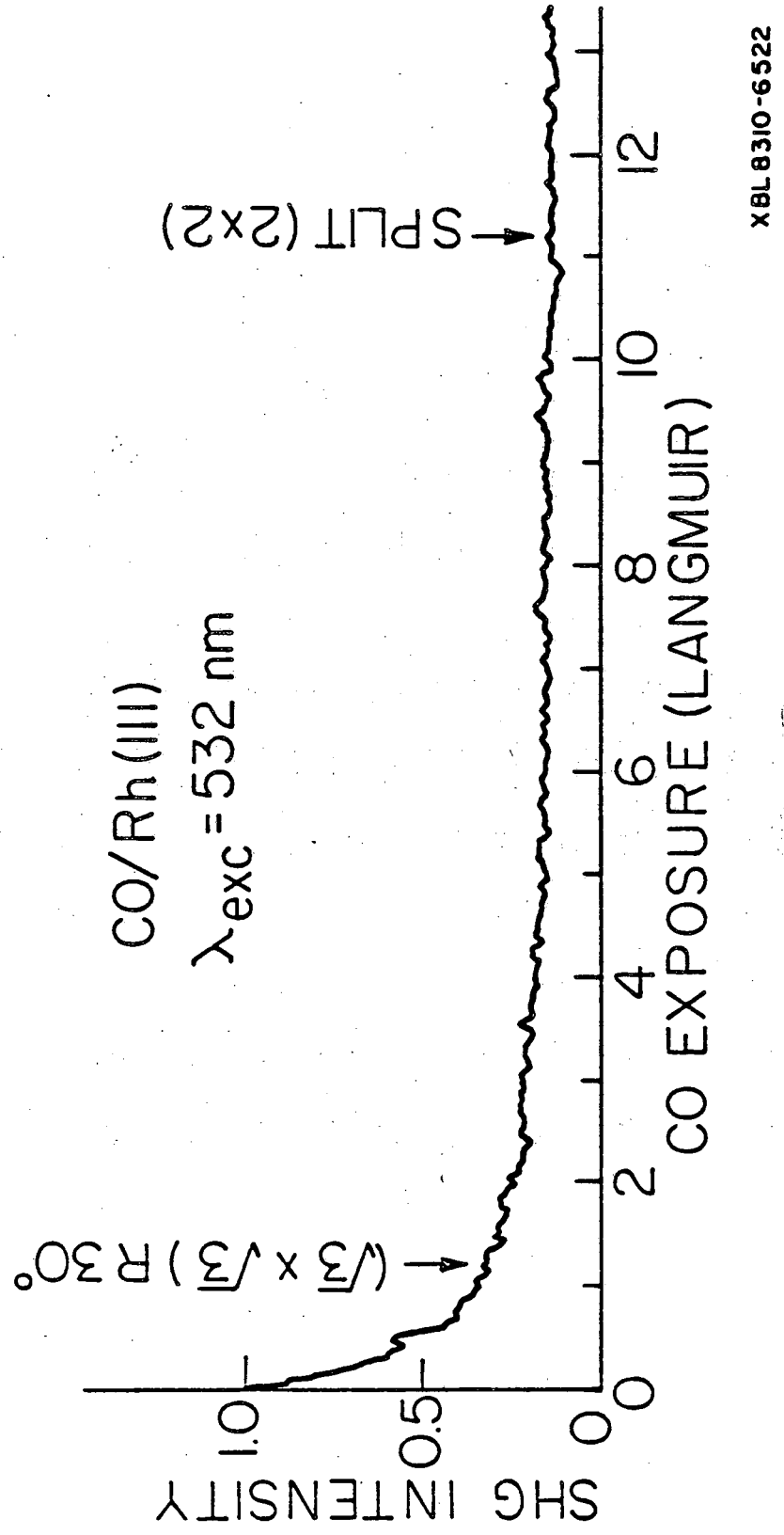
SHG INTENSITY
0.0
0.5
1.0
0
2
4
6
8
10
12
CO EXPOSURE (LANGMUIR)
CO/Rh(111)
λ_{exc} = 532 nm
(√3 x √3) R 30°
SPLIT (2x2)
XBL 8310-6522

Fig. 11(a)

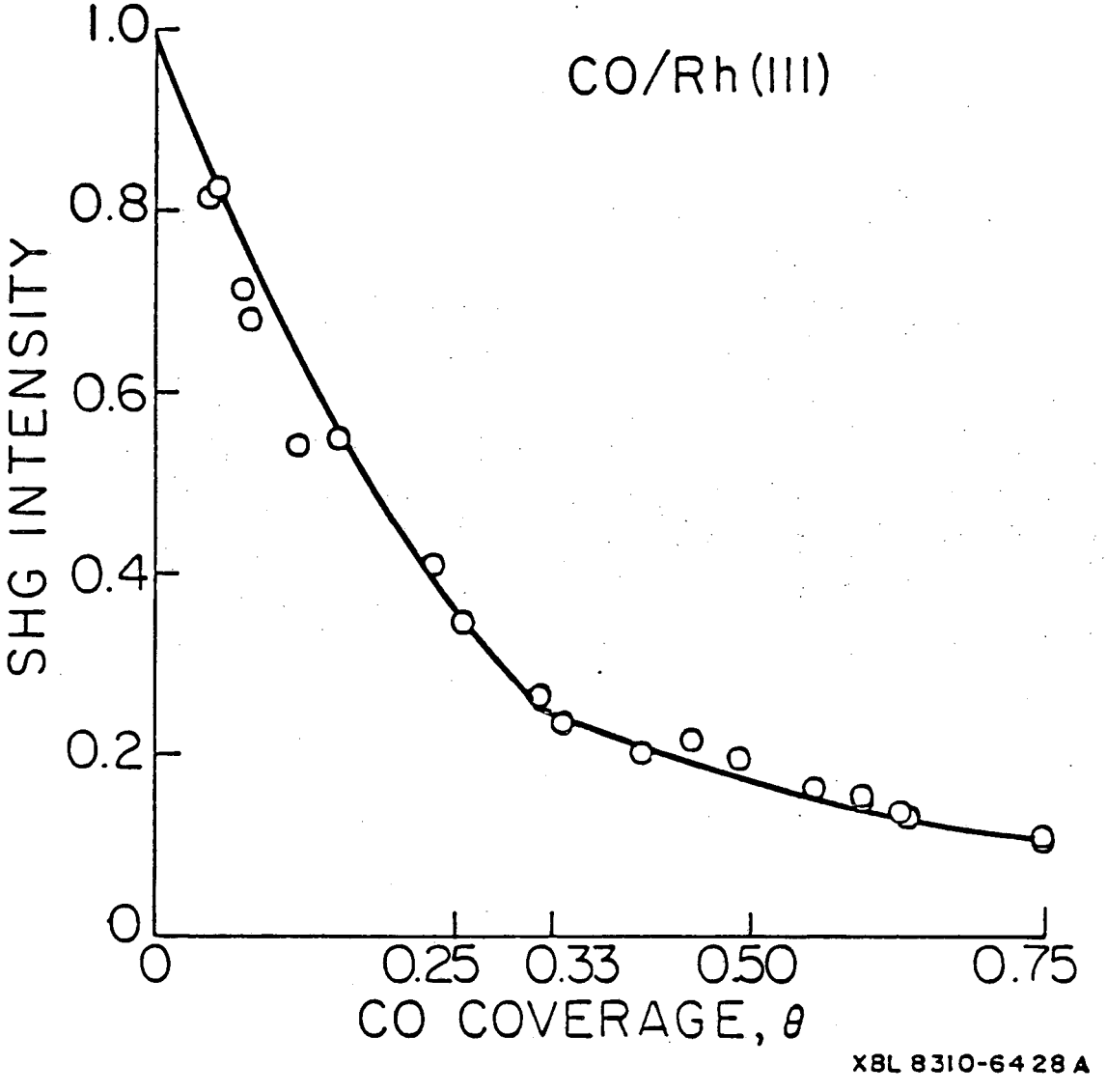
CO/Rh(111)
SHG INTENSITY
1.0
0.8
0.6
0.4
0.2
0
0
0.25
0.33
0.50
0.75
CO COVERAGE, θ
XBL 8310-6428A

Fig. 11(b)

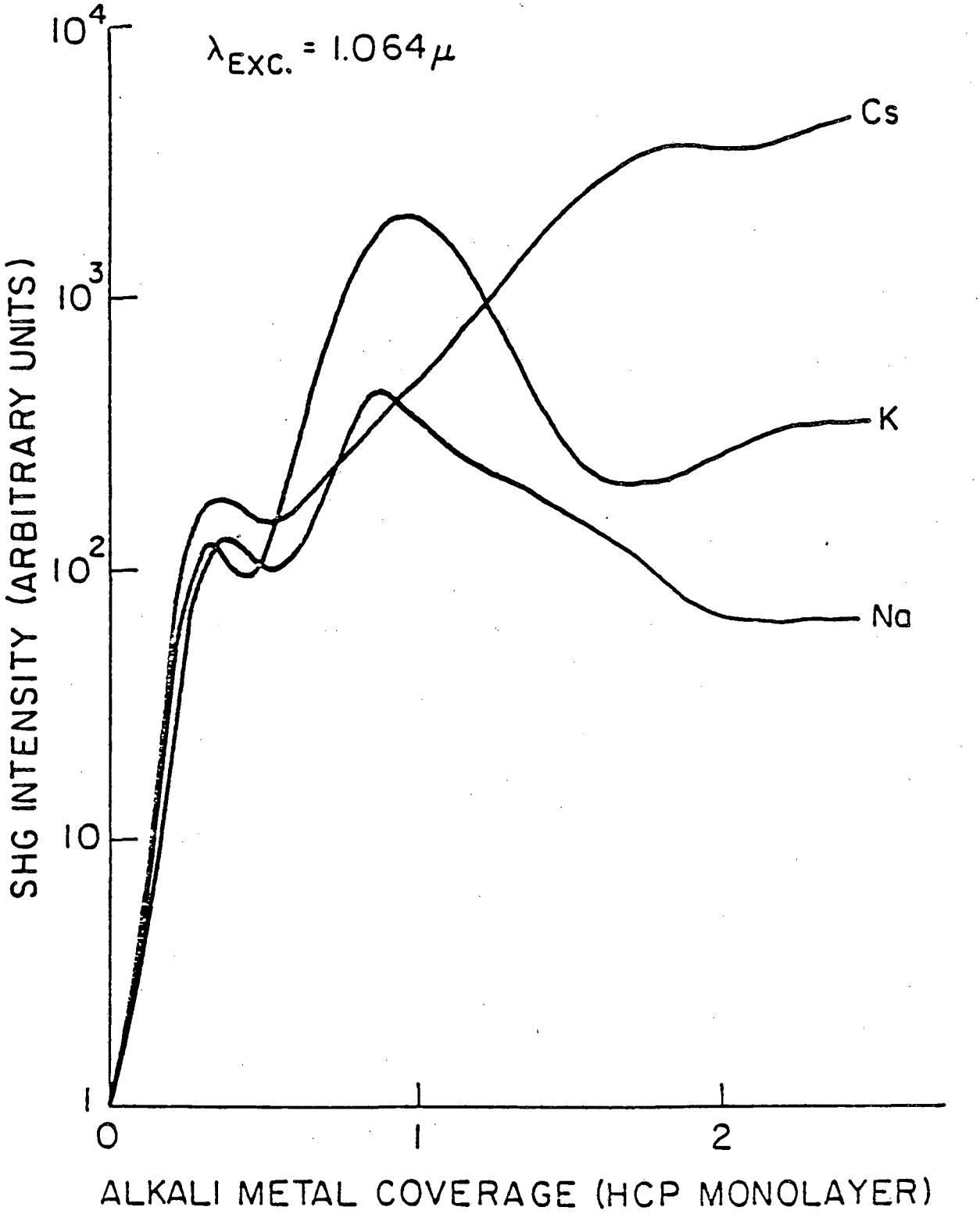
$\lambda_{EXC.} = 1.064\mu$
Cs
K
Na
SHG INTENSITY (ARBITRARY UNITS)
10^4
10^3
10^2
10
1
0
1
2
ALKALI METAL COVERAGE (HCP MONOLAYER)
XBL843-6722

Fig. 12

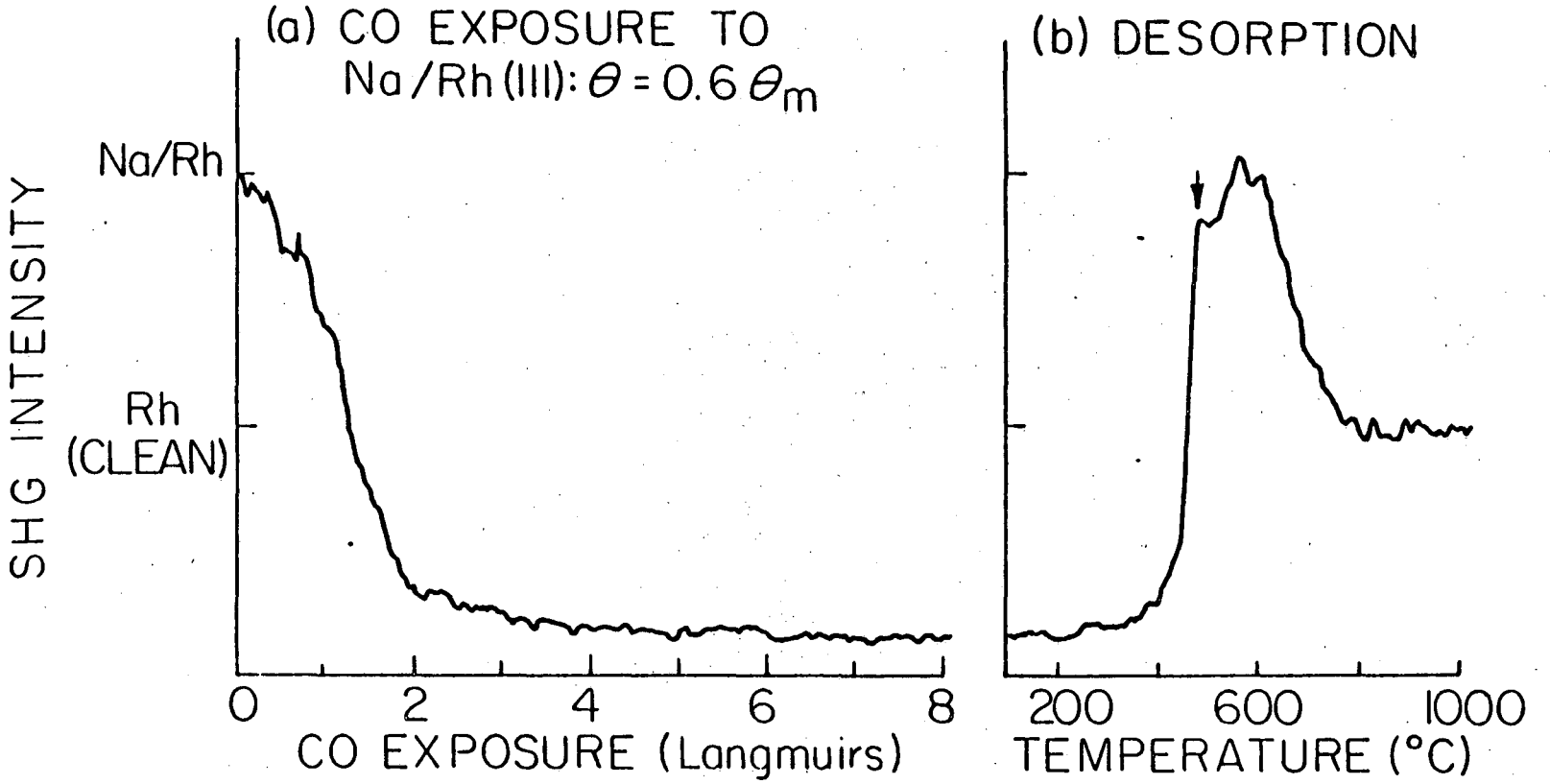

XBL 8310-6427A

Fig. 13

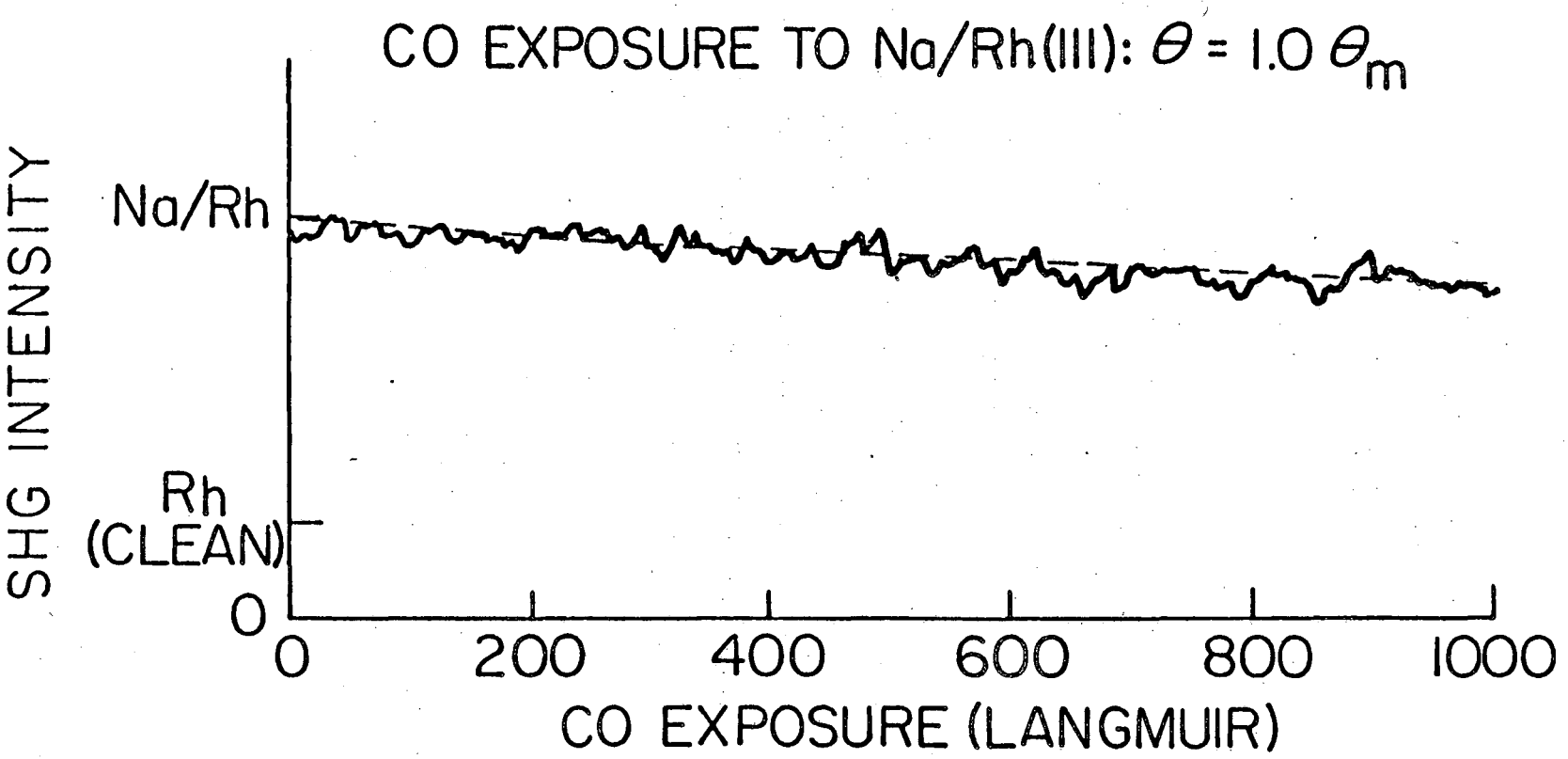
CO EXPOSURE TO Na/Rh(111): θ = 1.0 θm
SHG INTENSITY
Na/Rh
Rh
(CLEAN)
0
0
200
400
600
800
1000
CO EXPOSURE (LANGMUIR)
XBL8310-6523

Fig. 14

TECHNICAL INFORMATION DEPARTMENT
LAWRENCE BERKELEY LABORATORY
UNIVERSITY OF CALIFORNIA
BERKELEY, CALIFORNIA 94720